

Colon cancer cells colonize the lung from established liver metastases through p38 MAPK signalling and PTHLH

Jelena Urosevic^{1,8}, Xabier Garcia-Albéniz^{1,2,8}, Evarist Planet¹, Sebastián Real¹, María Virtudes Céspedes^{3,4}, Marc Guiu¹, Esther Fernandez¹, Anna Bellmunt¹, Sylwia Gawrzak¹, Milica Pavlovic¹, Ramon Mangués^{3,4}, Ignacio Dolado^{1,7}, Francisco M. Barriga¹, Cristina Nadal², Nancy Kemeny⁵, Eduard Batlle^{1,6}, Angel R. Nebreda^{1,6} and Roger R. Gomis^{1,6,9}

The mechanisms that allow colon cancer cells to form liver and lung metastases, and whether *KRAS* mutation influences where and when metastasis occurs, are unknown. We provide clinical and molecular evidence showing that different MAPK signalling pathways are implicated in this process. Whereas ERK2 activation provides colon cancer cells with the ability to seed and colonize the liver, reduced p38 MAPK signalling endows cancer cells with the ability to form lung metastasis from previously established liver lesions. Downregulation of p38 MAPK signalling results in increased expression of the cytokine PTHLH, which contributes to colon cancer cell extravasation to the lung by inducing caspase-independent death in endothelial cells of the lung microvasculature. The concerted acquisition of metastatic traits in the colon cancer cells together with the sequential colonization of liver and lung highlights the importance of metastatic lesions as a platform for further dissemination.

Colorectal cancer (CRC) metastasis follows an ordered and hierarchical pattern. CRC cells initially spread to the lymph nodes and peritoneal area. When metastases to the liver occur, a substantial number of patients develop also lung and less frequently bone or brain metastases¹. Patients with metastasis are treated with systemic chemotherapy, mostly in a palliative manner. Nevertheless, in selected patients with isolated liver metastasis, increased 5 year survival can be achieved by multimodal treatment that includes combination of surgery with modern chemotherapy². However, only about 25% of patients can benefit from this type of treatment and the presence of metastases in other organs is, in most cases, a contraindication for resection³. After liver, lung is the most frequently involved organ^{4,5}, which highlights the need to understand mechanisms of CRC lung metastasis to further improve disease control. The metastatic pattern in CRC could be partially explained by the fact that the gut-draining mesenteric vein together with the splenic vein forms the portal system that drains directly into the liver. Beyond this simplistic anatomical interpretation, mechanisms that regulate intravasation,

survival in portal circulation, infiltration and colonization of the liver are also likely to contribute to the propensity of CRC metastasis for the liver⁶. In addition, there is no explanation for why liver metastasis is accompanied by lung colonization only in some patients. Interestingly, CRC patients who underwent primary tumour resection show a different pattern of relapse depending on the *KRAS* mutational status⁷. In particular, *KRAS*-mutated CRC has a higher incidence of lung metastasis. This phenomenon suggests a *KRAS*-linked mechanism that favours targeting of colon tumour cells to the lungs⁸.

RESULTS

An experimental model of colon cancer metastasis

To investigate the hierarchical mechanisms of liver and subsequent lung metastasis in *KRAS*-mutated CRC, we established an orthotopic xenograft mouse model to select for human CRC cells with enhanced ability to colonize the liver and the lungs^{9,10}. We focused on the human colon adenocarcinoma cell line SW620, which harbours the *KRAS*^{G12V} mutation. First, we introduced in these cells an expression vector for

¹Institute for Research in Biomedicine (IRB Barcelona), 08028 Barcelona, Spain. ²Institut de Malalties Hemato-Oncològiques, Hospital Clínic de Barcelona-IDIBAPS and CIBER-EHD), 08036 Barcelona, Spain. ³Grup d'Oncogenesi i Antitumorals, Hospital de Sant Pau, 08026 Barcelona, Spain. ⁴Grup d'Oncogenesi i Antitumorals, Institute of Biomedical Research (IIB Sant Pau), Network Research Center on Bioengineering, Biomaterials and Nanomedicine (CIBER-BBN), 08026 Barcelona, Spain. ⁵Memorial Sloan-Kettering Cancer Center, 10065 New York, USA. ⁶Institució Catalana de Recerca i Estudis Avançats (ICREA), 08010 Barcelona, Spain.

⁷Molecular Partners AG, 8952 Schlieren, Switzerland. ⁸These authors contributed equally to this work.

⁹Correspondence should be addressed to R.R.G. (e-mail: roger.gomis@irbbarcelona.org)

luciferase, which allowed us to monitor the kinetics of emergence of liver metastatic lesions by quantitative bioluminescence imaging. The SW620 luciferase-expressing cells (parental) were inoculated into the portal circulation of immunodeficient mice through intrasplenic injection followed by splenectomy, to isolate cell populations that target the liver (Fig. 1a). The initial SW620-derived liver metastasis cells were expanded in culture and the resulting population (Liver Metastatic derivative, LiM1) was subjected to a second round of *in vivo* selection, producing the LiM2 cell population that showed a significant increase in liver metastatic activity (Fig. 1a–d). Within 10 weeks post inoculation of LiM2 cells, 15 out of 18 mice developed liver metastasis as opposed to 6 out of 18 injected with parental SW620 cells, suggesting that LiM2 cells acquired the ability to survive and adjust to the liver environment (Fig. 1b–d). Besides the increased ability to form liver metastasis, LiM2 cells also showed increased lung metastatic activity compared with parental SW620 cells (Fig. 1c,e), whereas peritoneal metastasis and ascites production were observed at lower but comparable rates in the two populations (Fig. 1c). Histological examination revealed that, in most cases, liver metastatic lesions derived from LiM2 cells developed stromal response, as opposed to the typical necrotic lesions derived from parental SW620 cells (Fig. 1d). Interestingly, LiM2 cells showed an increased invasive capacity *in vitro* compared with parental cells, suggesting the potential gain of metastatic features (Supplementary Fig. 1a). Furthermore, LiM2 cells also showed enhanced liver and lung metastatic capabilities in orthotopic mouse xenografts, whereas primary tumours grew similarly to the parental cell population, indicating that proliferation was not enhanced in LiM2 cells by the *in vivo* selection protocol (Supplementary Fig. 1b–d).

Deregulated MAPK signalling in colon cancer cells is associated with metastatic capacity

To investigate the molecular basis for aggressive concerted liver and lung metastatic behaviour of *KRAS*-mutated CRC cells, we performed transcriptomic analysis of the LiM2 and parental SW620 cell populations. Comparative genome-wide expression analysis yielded a list of 194 genes that were overexpressed or underexpressed at least 2.5-fold in the highly liver metastatic derivative LiM2 (Fig. 2a and Supplementary Table 1). This group of genes showed a concordant trend of regulation in metastatic derivatives and was named the colon cancer metastatic (CCM) gene set. We divided the CCM set of genes in two groups depending on whether their expression was upregulated or downregulated, and performed a cross-validation in a combined expression data set of 267 stage I–III clinically annotated human primary CRC tumours from three independent institutions (combined GSE17537 and GSE14333) (refs 11–13). The outcome of interest was time to recurrence after primary tumour retrieval. Using gene set enrichment analysis¹⁴ (GSEA), we found a strong association between the upregulated CCM gene set and an increased risk of recurrence (hazard ratio, HR) on treatment (false discovery rate $<1 \times 10^{-6}$) (Fig. 2b). In contrast, the downregulated CCM gene set was not found to be significantly associated with reduced risk of recurrence (Supplementary Fig. 2a). Similar conclusions were obtained using GSE17537 and GSE14333 expression data sets independently. Survival analysis establishing subgroups by the median expression of the upregulated CCM gene set also revealed that this gene set was

associated with reduced time to recurrence (Fig. 2b). Patients in the combined GSE17537 plus GSE14333 cohort with higher expression of the CCM gene set had an increment of 120% in the rate of recurrence along time (HR = 2.20, 95% CI 1.22–3.98, $P = 0.007$). Stage- and study-adjusted multivariate analysis yielded a HR of similar magnitude (HR = 1.88, 95% CI 1.04–3.36, $P = 0.037$) supporting the independent predictive capacity of the upregulated CCM gene set.

The integration of different oncogenic hits into particular signalling pathways and cellular functions is key to understand how the expression of groups of genes is collectively changed in metastatic cell populations. Thus, we investigated the signalling pathways predicted to regulate the expression of genes associated with increased metastatic capacity of LiM2 cells. By using BGSEA (ref. 14), we found several pathway-specific gene expression signatures (KEGG gene sets) that were differentially represented in the gene expression profiles of parental and LiM2 cells (Fig. 2c and Supplementary Table 2). These included the pathways of nitrogen metabolism, which supports nucleotide synthesis, cell adhesion molecules, which are fundamental for invasion and migration, and mitogen-activated protein kinases (MAPKs), which are important modulators of cellular responses¹⁵ (Supplementary Table 2). We focused our attention on MAPK signalling alterations given the *KRAS*-mutated status of our initial CRC cell population. We analysed the activation status of the three main MAPK pathways in LiM2 cells and found that the activating phosphorylation of ERK1/ERK2 was increased, whereas that of p38 MAPKs was reduced (Fig. 2d and Supplementary Fig. 2b) and the phosphorylation of JNKs did not change (Fig. 2d). Significantly, when the relative levels of phosphorylated (active) ERK2 and ERK1 were compared, we found that phospho-ERK2 levels were specifically increased over phospho-ERK1 in CRC tumour biopsies from patients that developed metastasis within 2 years post-surgery compared with healthy mucosa from the same patients (distance from the tumour >10 cm) or to CRC tumours of patients free of metastasis (Fig. 2e). In 6 out of 7 primary tumours from CRC patients that developed metastasis, the phospho-ERK2/phospho-ERK1 ratio was above 1, whereas only 3 out of 13 non-metastatic CRC primary tumours had higher phospho-ERK2 than phospho-ERK1 levels (Fig. 2e, $P = 0.036$). Furthermore, in a set of 20 healthy mucosa samples obtained from the same patients as the CRC primary tumours, phospho-ERK2 levels were roughly equal to those of phospho-ERK1 in 80% of the samples similarly to non-metastatic CRC primary tumours (Fig. 2e). Next, we investigated the implication of the p38 MAPK pathway, which was downregulated in LiM2 cells, and found that the reduced levels of phosphorylated (active) p38 MAPK correlated with the downregulation of MKK6 (*MAP2K6*), a key activator of p38 MAPKs (ref. 16; Fig. 2f). Notably, in CRC primary tumours (pooled GSE17537 and GSE14333; $n = 267$ including stages I, II and III), *MKK6* messenger RNA expression levels were inversely associated with a high probability of relapse in the patients (Fig. 2g). These results support that high phospho-ERK2 and low phospho-p38 MAPK activities are associated with risk of metastasis in CRC patients.

ERK2 mediates colon cancer metastasis to the liver

Given that lung and liver metastatic events are co-selected in CRC patients (Supplementary Table 3), particularly bearing *KRAS*-mutated tumours, we wondered whether concerted changes in signalling

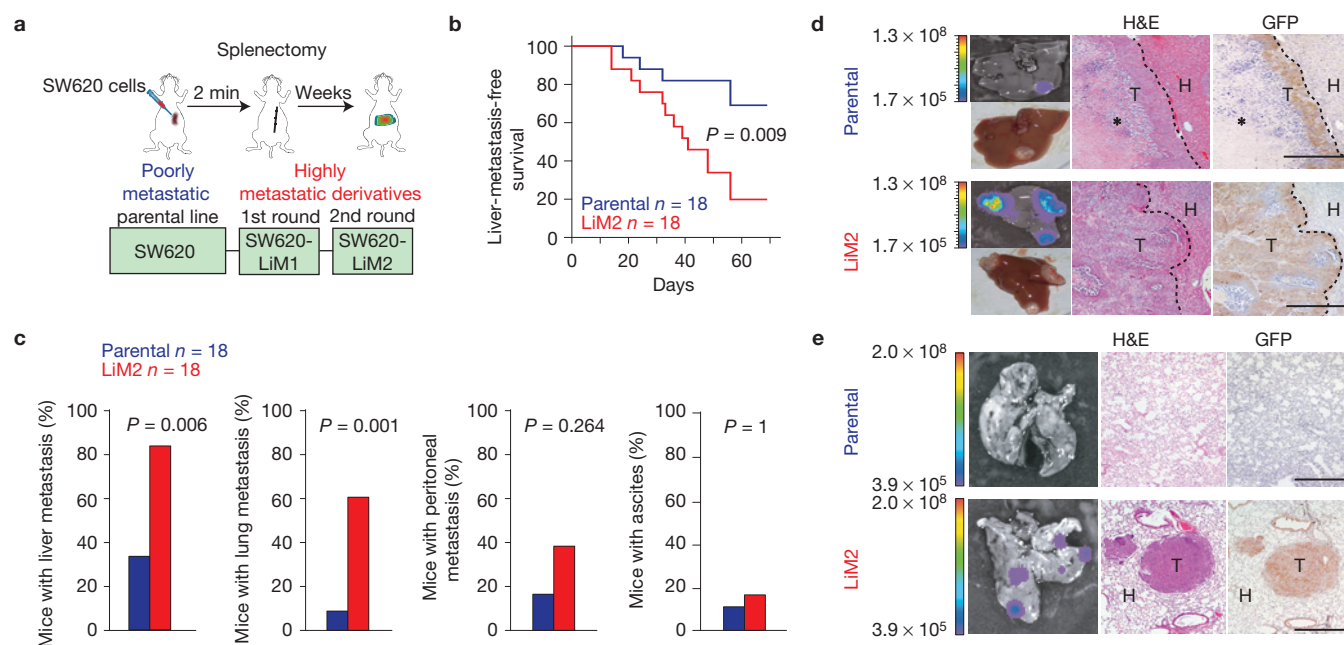


Figure 1 Isolation and characterization of liver metastatic derivatives from SW620 *KRAS*-mutated colorectal cancer (CRC) cells. **(a)** Schematic representation of *in vivo* selection and isolation of liver metastatic derivatives. **(b)** Liver-metastasis-free survival of mice injected intrasplenically with SW620 poorly metastatic (parental) or highly metastatic (LiM2) cells. $n = 18$ mice (pooled from two independent experiments) used per cell line. Log-rank test was used to determine statistical significance. **(c)** Percentage of liver metastasis, lung metastasis, peritoneal metastasis and ascites in mice on intrasplenic injections of SW620 parental

and LiM2 cells determined post-mortem. Results were obtained using 18 mice (n) per cell line, and two-sided Fisher's exact test was used to calculate statistical significance. **(d)** Representative bioluminescent images and photographs of livers, and haematoxylin and eosin (H&E) and GFP staining of the liver sections. Scale bars, 500 μm . H, healthy tissue; T, tumour; *, necrotic area. **(e)** Representative bioluminescent images of lungs, and H&E and GFP staining of the lung sections from mice injected intrasplenically with SW620 parental and LiM2 cells. Scale bars, 500 μm .

pathways might be responsible for lung and liver colonization. Thus, we next evaluated the contribution of each MAPK signalling pathway to *KRAS*-mutated CRC liver and lung metastasis. As ERK2 activation was increased in primary tumours of patients that developed metastases, we downregulated the expression of ERK2 or ERK1 in LiM2 cells by means of two independent short hairpin RNAs (shRNAs; Fig. 3a and Supplementary Fig. 3a) Importantly, ERK2-knockdown significantly decreased the capacity of LiM2 cells to colonize the liver on intrasplenic injection into nude mice (Fig. 3a,b) whereas ERK1-knockdown had no effect (Supplementary Fig. 3b). Of note, neither ERK2 nor ERK1 depletion caused significant differences in orthotopic tumour growth, proliferation or apoptosis (Supplementary Fig. 3c–e). Interestingly, ERK2, but not ERK1, has been proposed to regulate, through changes in expression of the transcription factors *FRA1* and *ZEB1*, a set of epithelial to mesenchymal transition responses in breast cancer cells¹⁷, which has been associated with metastatic behaviour⁶. We confirmed that high *FRA1* expression levels were associated with relapse in the combined colon cancer primary tumour gene expression cohort described above (Supplementary Fig. 3f). These results support that ERK2 signalling drives liver metastasis in *KRAS*-mutated CRC cells.

p38 MAPK signalling mediates colon cancer metastasis to the lung

Unexpectedly, ERK2 downregulation did not affect the capacity of *KRAS*-mutated CRC cells to colonize the lungs (Fig. 3b). Thus, we

reasoned that lung colonization was controlled by an independent mechanism. The p38 MAPK pathway has been implicated in several pro and anti-tumorigenic functions¹⁵ and we found that human fresh CRC tumour biopsies with low phospho-p38 MAPK levels were associated with metastasis to lung but not to other tissues (Supplementary Fig. 4a). To test the potential contribution of this pathway to CRC metastasis to the lung, we used the p38 MAPK specific inhibitor PH-797804 (ref. 18). Parental cells were implanted directly into the liver of nude mice (one implant per mouse) and, when liver tumour photon flux signal reached a certain value ($> 10^8$ photons s^{-1}), mice were randomly allocated to daily systemic treatment with either vehicle or PH-797804 (Fig. 3c). Fifteen days post treatment, an increase in lung metastatic events was observed in PH-797804-treated mice, whereas liver tumour growth was similar in both groups of mice (Fig. 3c). Histological analysis confirmed p38 MAPK inhibition in PH-797804-treated mice (Fig. 3c). As an alternative experimental setting to test the implication of the p38 MAPK pathway in liver and lung metastasis from the primary colon tumour, we used HCT116 cells. These *KRAS*-mutated CRC cells have the ability to form liver and lung metastasis when implanted orthotopically in nude mice as opposed to SW620 parental cells, which mainly produced lymph node metastasis¹⁹ (Supplementary Fig. 1). We generated two derivatives of HCT116 cells expressing either shRNA to downregulate p38 α (Fig. 3d), the most abundant p38 MAPK family member, or MKK6^{EE} to constitutively activate the p38 MAPK pathway¹⁶. The two cell populations together with parental HCT116 cells were implanted

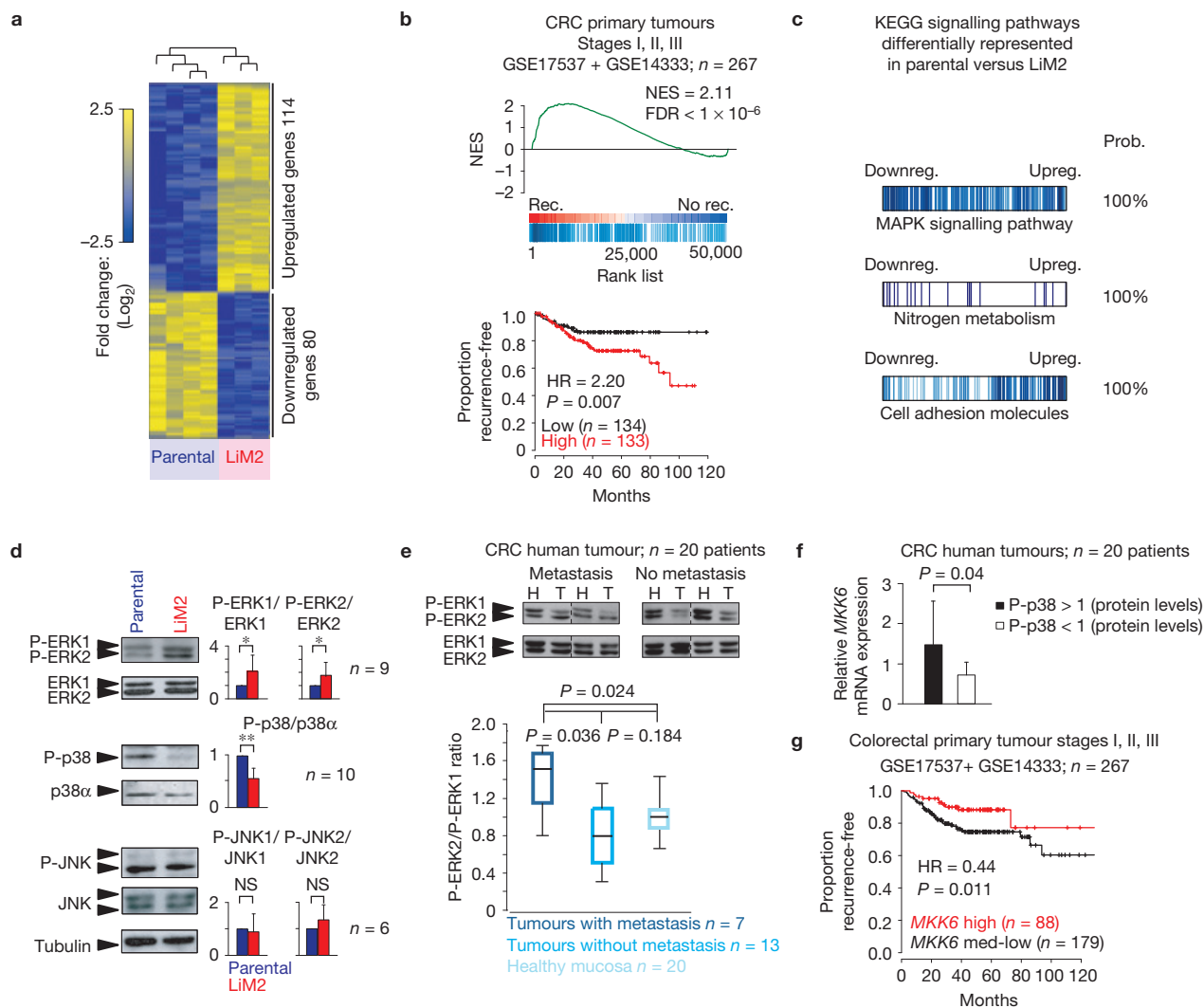


Figure 2 Liver metastatic derivatives from SW620 *KRAS*-mutated CRC cells present changes in MAPK signalling pathways. **(a)** Heat map representing differential gene expression pattern between parental and LiM2 cells, using 2.5-fold change as a cutoff. 114 genes were found upregulated (yellow) and 80 downregulated (blue) in LiM2 compared to parental cells. **(b)** Gene set enrichment analysis (GSEA; top) and Kaplan–Meier plot (bottom) representing association of HR of recurrence with the upregulated CCM gene set in the human colon cancer data set (pooled GSE17537 and GSE14333; $n = 267$). NES, normalized enrichment score; FDR, false discovery rate; HR, hazard ratio. **(c)** KEGG analysis representing signalling pathways differentially represented in parental and LiM2 cells. **(d)** Left: Western blot of phosphorylated ERK1/2, p38 and JNK MAPKs (P-ERK1/2, P-p38, P-JNK) in SW620 parental and LiM2 cells. Total protein levels of ERK1/2, p38 and JNK were analysed. Tubulin was used as a loading control. Right: Quantification of phosphorylated ERK1/2, p38 and JNK MAPKs normalized to total amount of the same proteins. $n = 9$ (ERK1/2), $n = 10$ (p38) and $n = 6$ (JNK) biological replicates pooled from at least three independent experiments. Plots represent average plus s.d. $*P < 0.05$;

$**P < 0.001$; NS, not significant. **(e)** Top: Levels of phosphorylated ERK1/2 (P-ERK1/2) and total ERK1/2 proteins were analysed in samples of 20 primary CRC tumour samples (T) and their respective healthy mucosa (H) by western blotting and representative blots are shown. The dashed lines separate representative patient samples spliced from different gels. Bottom: Ratio of P-ERK2/P-ERK1 normalized to total amount of protein in samples of CRC tumours determined by western blotting; $n = 7$ tumours with metastasis, $n = 13$ tumours without metastasis, $n = 20$ healthy mucosa. Statistics: two-tailed Mann–Whitney test; the box: 25th–75th percentile where the black line within the box represents the median; whiskers: 10th–90th percentile. **(f)** Association of *MKK6* mRNA levels with the ratio of phosphorylated p38 (P-p38) protein levels in CRC tumours from $n = 20$ patients. Plots represent average plus s.d. **(g)** Kaplan–Meier curves representing the proportion of recurrence-free patients stratified according to *MKK6* mRNA levels in CRC patient samples (pooled GSE17537 and GSE14333; $n = 267$). Statistical analysis was done using Cox proportional hazard’s model in **b** and **g**, and two-tailed Student’s *t*-test in **d** and **f**. Uncropped images of blots are shown in Supplementary Fig. 8.

orthotopically into the caecum, intestinal wall, of nude mice and 4 months later the mice were euthanized and primary tumours and metastatic lesions to the liver and lungs were quantified. No differences in proliferation and apoptosis rates in the primary tumours were detected among the groups (Supplementary Fig. 4b). Histological analysis of the number and area of liver metastasis showed no

significant differences between control and p38 α -knockdown cell populations, whereas the percentage of mice with liver metastasis was decreased in the latter group (Supplementary Fig. 4c,d). Interestingly, HCT116 cells with reduced levels of p38 α showed a significantly higher capacity to colonize the lungs (Fig. 3d). Conversely, activation of the p38 MAPK pathway by expression of MKK6^{EE} markedly

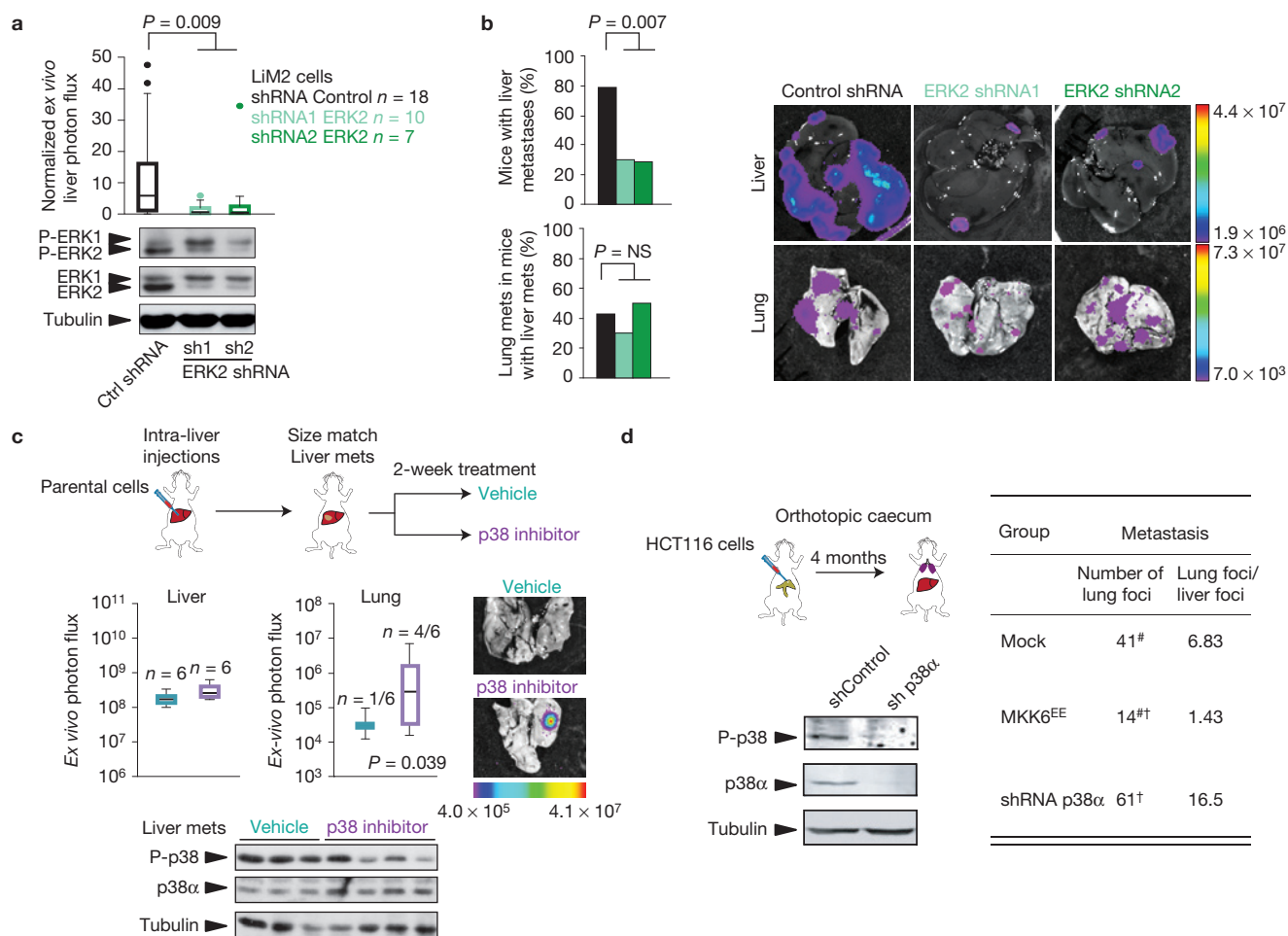


Figure 3 MAPK pathways mediate liver and lung metastasis in CRC. **(a)** Top: Normalized ex vivo liver photon flux of mice injected intrasplenically with LIM2 cells expressing control shRNA or two different ERK2 shRNAs. Bottom: ERK2 downregulation was confirmed by western blot analysis; $n = 18$ (Control shRNA), $n = 10$ (ERK2 shRNA1) and $n = 7$ (ERK2 shRNA2) mice used in each group pooled from two independent experiments. Statistical significance was calculated using two-tailed Mann–Whitney test; the whiskers extend from min. to max. of 1.5 interquartile range (Tukey box plot). **(b)** Percentage of mice intrasplenically injected with LIM2 cells expressing the indicated shRNAs that developed liver metastasis (top) or lung metastasis (bottom). Representative bioluminescent images of livers and lungs are shown; n , number of mice used in each group is stated in **a**; statistical significance was calculated using two-sided Fisher's exact test. NS, not significant. **(c)** Top: SW620 parental cells were injected intra-liver and when lesions reached a size of $>10^8$ photons s^{-1} , mice were randomly separated into groups for two-week treatment with vehicle ($n = 6$) or the p38 MAPK inhibitor PH-797804 ($n = 6$). Ex vivo liver and lung photon flux of the 2 groups of mice together

with representative bioluminescent images of lungs are shown. One-sided chi-squared test was used to calculate statistical significance. The whiskers extend from the 10th to 90th percentile. Bottom: Western blot analysis of P-p38 MAPK and p38 α protein levels in metastatic lesions on two-week treatment with vehicle or PH-797804. **(d)** Left: Western blot analysis of P-p38 MAPK and p38 α levels in HCT116 cells infected with lentivirus expressing the indicated shRNAs. HCT116 cells expressing p38 α shRNAs or constitutively active MKK6^{EE} were injected orthotopically into mice caecum, and the number of lung foci and the ratio between the number of lung and liver foci was determined. $n = 5$ (Mock), $n = 5$ (MKK6^{EE}) and $n = 4$ (p38 α shRNA) mice that developed lung metastasis in each group. [#] $P = 0.043$, [†] $P = 0.031$ indicate statistical significance between the groups. Statistical significance was calculated using one-tailed Mann–Whitney test. In **a** and **c** the box extends from the 25th to 75th percentile and the black line within the box represents the median. Uncropped images of blots are shown in Supplementary Fig. 8. Representative western blot images in **a** and **d** from three independent experiments.

reduced the ability of HCT116 cells to colonize the lungs, without changing the liver colonization capacity (Fig. 3d and Supplementary Fig. 4c,d). Collectively, these results suggest that the p38 MAPK pathway negatively regulates the ability of KRAS-mutated CRC cells to metastasize to the lung without affecting liver colonization.

p38 MAPK signalling controls PTHLH expression in metastatic colon cancer cells

Next we investigated the mechanism by which p38 MAPK signalling may drive lung metastasis from a previously established liver

metastasis. First, we excluded any differences in apoptosis rates of metastatic emerging colonies due to variations in p38 MAPK activity in HCT116 or SW620 cell derivatives (Supplementary Fig. 4e,f). Next, we focused on genes under the control of this pathway that could potentially interact with the liver or lung stroma to trigger lung colonization. Among the genes that correlated with MKK6 expression levels in CRC primary tumours ($p < 0.05$) and whose expression changed at least 1.7-fold in metastatic LIM2 over parental SW620 cells, the parathyroid hormone-like hormone (PTH_{LH}) captured our attention as a gene that was upregulated

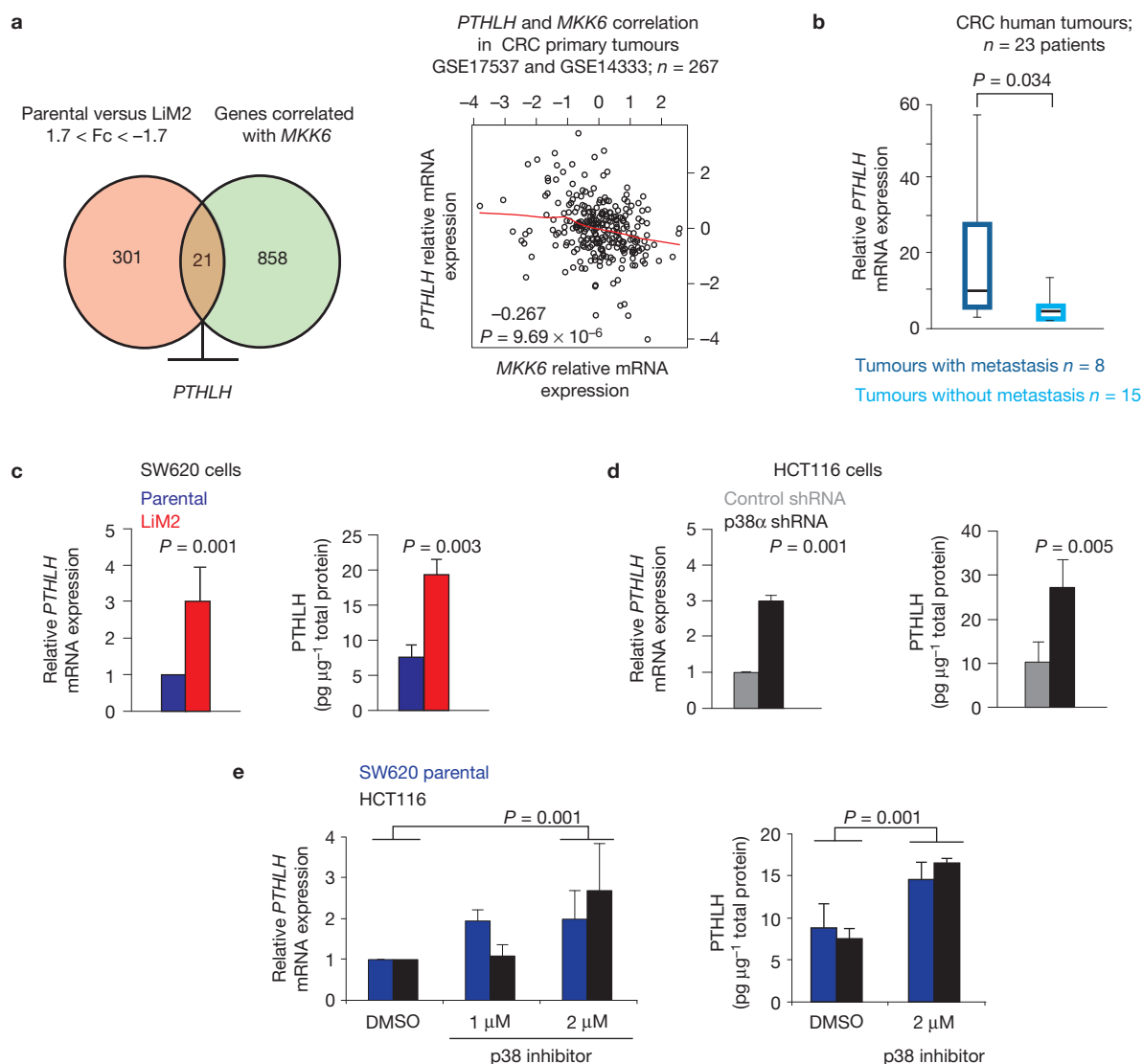


Figure 4 p38 MAPK pathway controls the expression of *PTHLH* cytokine. (a) Left: Venn diagram showing the overlap between genes that are differentially expressed in parental and LiM2 cells (cutoff 1.7), orange group, and genes that correlate significantly with *MKK6* expression in CRC primary tumour set GSE14333 (stages II and III), green group. Right: *PTHLH* and *MKK6* Spearman correlation in CRC primary tumours (GSE17537 and GSE14333; $n = 267$). (b) qRT-PCR analysis of *PTHLH* mRNA levels in CRC primary tumours that developed or did not develop metastases; $n = 8$ tumours with metastasis and $n = 15$ tumours without metastasis. The box extends from the 25th to 75th percentile and the black line within the box represents the median; the whiskers extend from the 10th to 90th percentile. (c) mRNA and protein levels analysis of *PTHLH* in SW620 parental

and LiM2 cells. $n = 3$ values per group from independent experiments. Plots represent average plus s.d. (d) mRNA and protein levels of *PTHLH* in extracts of HCT116 cells infected with lentivirus expressing the indicated shRNAs. $n = 3$ values per group for mRNA studies and $n = 4$ values per group for protein studies. Each value is obtained in independent experiments. Plots represent average plus s.d. (e) mRNA and protein levels of *PTHLH* in SW620 parental and HCT116 cells treated with the indicated doses of the p38 MAPK inhibitor PH-797804. $n = 4$ (SW620 parental) and $n = 3$ (HCT116) for mRNA studies. $n = 3$ values per group for protein studies. Each value is obtained in an independent experiment. Plots represent average plus s.d. Statistical analysis was done using two-tailed Student's *t*-test in **b–e**.

(3.3-fold) and capable of conducting cancer cell–stroma interactions (Fig. 4a and Supplementary Table 4). The association of high *PTHLH* expression levels with metastatic relapse was confirmed in the combined primary tumour gene expression cohort described above (Supplementary Fig. 5a). We further validated the association of high risk of metastasis with increased levels of *PTHLH* in an independent set of 23 CRC tumour samples, including normal mucosa from the same patients (Fig. 4b). Previous reports have implicated *PTHLH* in endochondral bone development and epithelial–mesenchymal

interactions^{20,21} although, so far, it has never been associated with lung metastasis. Importantly, *PTHLH* was upregulated not only in highly metastatic LiM2 cells but also in p38 α -knockdown HCT116 cells and in p38 MAPK inhibitor treated SW620 parental and HCT116 cells (Fig. 4c–e and Supplementary Fig. 5b,c).

PTHLH as mediator of lung metastasis extravasation

To test the implication of *PTHLH* in lung metastasis of *KRAS*-mutated CRC cells, we downregulated *PTHLH* protein in highly metastatic

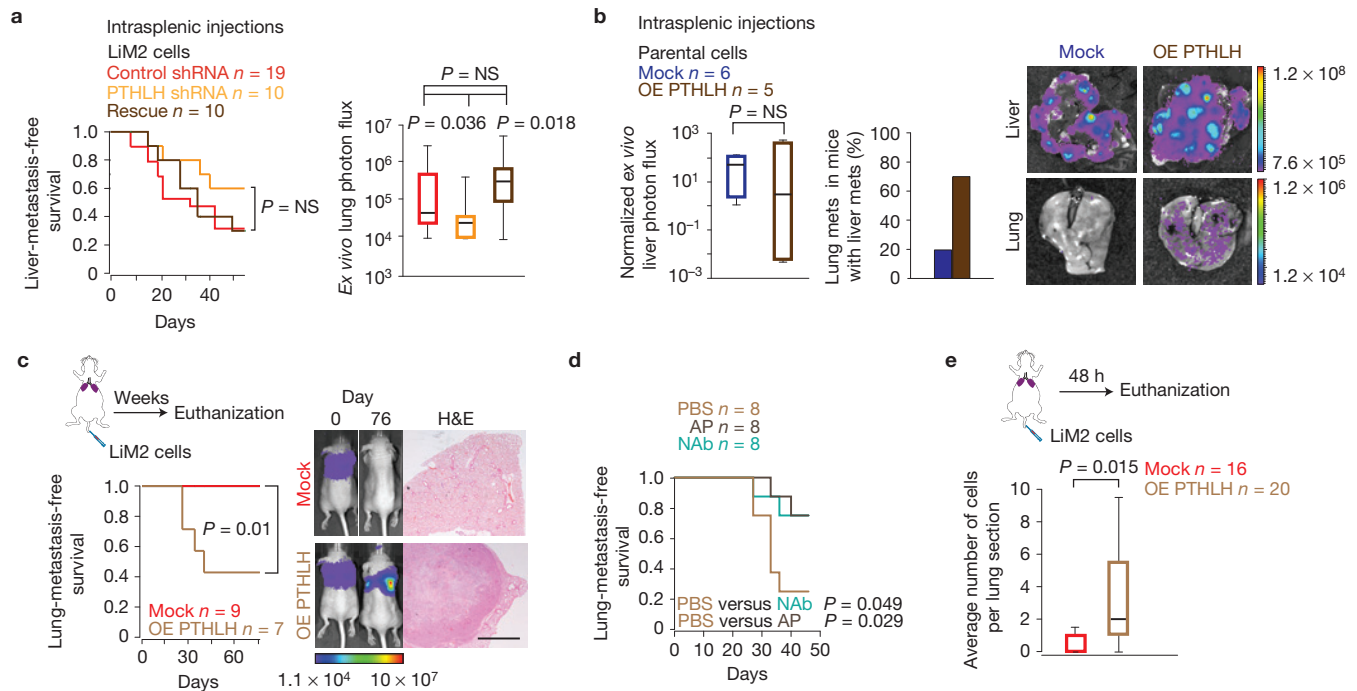


Figure 5 PTHLH controls CRC metastasis to the lung. **(a)** Left: Liver-metastasis-free survival curve of mice injected intrasplenically with LiM2 cells infected with lentivirus expressing control shRNA or PTHLH shRNA and with cells in which PTHLH shRNA was combined with exogenous expression of PTHLH (rescue). Right: *Ex vivo* lung photon flux in mice injected intrasplenically with the above mentioned cell lines; $n=19$ (control shRNA), $n=10$ (PTHLH shRNA) and $n=10$ (rescue) number of mice used in each group pooled from two independent experiments; for *ex vivo* lung photon flux statistics was calculated using one tailed Mann–Whitney test. NS, not significant. **(b)** Left: Normalized liver *ex vivo* photon flux on intrasplenic injections of SW620 parental cells either mock infected or infected with a retrovirus that expresses PTHLH. Percentage of lung metastasis in mice that developed liver metastasis on intrasplenic injection of the indicated cells; $n=6$ (mock) and $n=5$ (overexpressing (OE) PTHLH) number of mice used in each group. Right: Representative bioluminescent images of liver and lung metastatic lesions. **(c)** Left: Lung-metastasis-free

survival on tail vein injections of control LiM2 cells (mock) or PTHLH-expressing LiM2 cells (OE PTHLH). $n=9$ (mock) and $n=7$ (OE PTHLH) mice used in each group. Right: Representative bioluminescent images of mice at days 0 and 76 on injection and representative H&E staining of lung sections are shown. Scale bar, $500\mu\text{M}$. **(d)** Lung-metastasis-free survival on tail vein injections of PTHLH-expressing LiM2 cells treated with PBS, PTHLH-neutralizing antibody (+NAb) or antagonist PTHLH peptide (+AP). $n=8$ (PBS), $n=8$ (AP) and $n=8$ (NAb) number of mice used in each group. **(e)** Average number of cells found per lung section 48 h after tail vein injection of LiM2 cells either mock infected or overexpressing PTHLH. Four $30\mu\text{m}$ distant sections per animal were counted. $n=16$ (mock) and $n=20$ (OE PTHLH) total number of sections counted per group. In **a**, **b** and **e** the box extends from the 25th to 75th percentile and the black line within the box represents the median; whiskers: 10th to 90th percentile. Statistics: **a** left, **c** and **d** log-rank test; **b** and **e** two-tailed Mann–Whitney test.

LiM2 cells (Supplementary Fig. 5d). We found that PTHLH-deficient LiM2 cells were not significantly affected in liver metastatic activity (Fig. 5a) but had decreased ability to form lung metastasis in mice (Fig. 5a). On the other hand, PTHLH downregulation did not affect the growth of LiM2 cells directly implanted in the lung parenchyma of nude mice, indicating a possible role for PTHLH in the process of lung metastatic extravasation (Supplementary Fig. 6a,b). Importantly, PTHLH overexpression sufficed to provide SW620 parental cells with the ability to efficiently colonize lungs from the liver irrespectively of p38 MAPK activity levels (Fig. 5b). We reasoned that a constant and continuous release of PTHLH from an established liver metastasis could be necessary for priming the lung before colonization. Consistent with the idea that distant preparation of the niche might precede colonization, LiM2 cells were not able to colonize the lung when delivered to the mice through the tail vein (Supplementary Fig. 6c). Interestingly, LiM2 cells overexpressing large quantities of PTHLH were capable of lung colonization when injected into mice through the tail vein bypassing the requirement for the existence of a pre-established liver metastatic lesion (Fig. 5c). This

was dependent on PTHLH because interfering with this cytokine, by systemic administration of either a neutralizing antibody or an antagonist peptide, impaired the lung colonization process (Fig. 5d). As this experimental model is largely dependent on the extravasation capabilities of metastatic cells and no significant differences were observed in invasion, survival and migration functions, we tested the contribution of PTHLH to cancer cell extravasation at the lung. LiM2 cells overexpressing or not PTHLH, were injected through the tail vein and mice were euthanized 48 h later. Subsequently, lungs were extracted and the amount of cells extravasated into the lung parenchyma was determined. This experiment showed a fivefold increase in the number of cells detected per lung section in mice injected with PTHLH-overexpressing LiM2 cells (Fig. 5e). Similar results were obtained using an *in vitro* surrogate assay based on the migration of LiM2 cells through a monolayer of endothelial cells (Supplementary Fig. 7a).

To understand how the PTHLH released from tumour cells supports extravasation, tight monolayers of human pulmonary endothelial cells (HPMEC), which express the PTHLH receptor

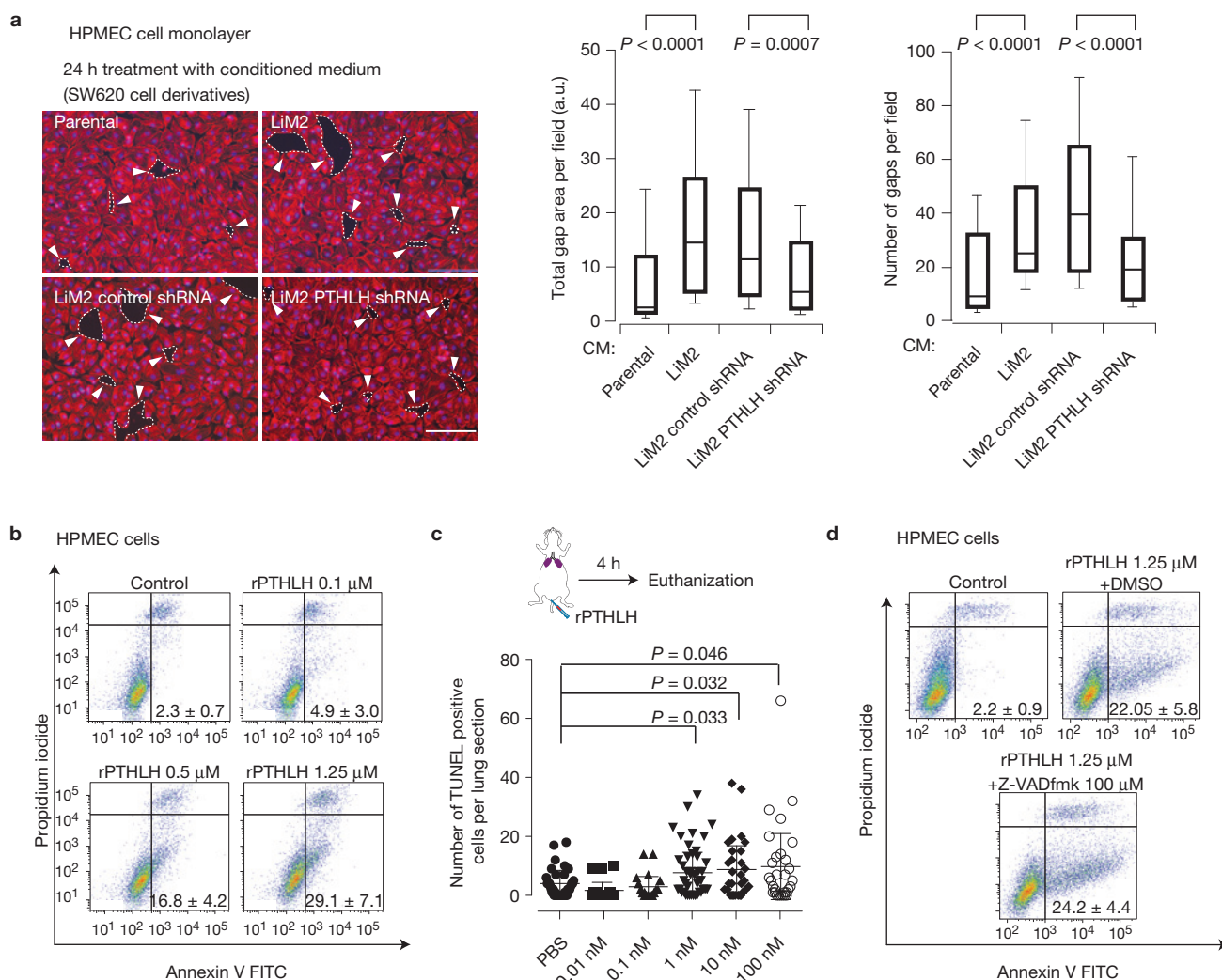


Figure 6 PTHLH induces caspase-independent death of human lung vasculature endothelial cells. **(a)** Left: HPMEC cells were grown until reaching tight confluence and then were treated with SW620 parental, LiM2, LiM2 control shRNA and LiM2 PTHLH shRNA cells conditioned medium for 24 h. Next, phalloidin (red) and DAPI (blue) stainings were performed. Gaps that are formed in the monolayer on conditioned media treatment are indicated with arrowheads and delineated with dashed lines. Scale bar, 200 μm . Right: Total gap area and number of gaps per field were determined. Results represent three independent experiments where each sample was seeded in duplicate and at least ten fields per coverslip were analysed (gap area: $n=64, 85, 86$ and 77 fields per group were analysed, respectively; and gap number: $n=63, 85, 66$ and 78 fields per group were analysed, respectively). Statistical significance was calculated using two-tailed Student's *t*-test; the box extends from the 25th to 75th percentile and the black line within the box represents the median; the whiskers extend from the 10th to 90th percentile.

(b) Annexin V flow cytometry analysis of HPMEC cells treated for 4 h with the indicated concentrations of PTHLH. **(c)** Average number of TUNEL-positive endothelial cells in lungs 4 h post tail vein injection of recombinant PTHLH (1–34). At least four 30 μm distant sections per animal were counted. PBS ($n=47$ sections; 10 mice), 1 nM rPTHLH ($n=48$ sections; 10 mice), 0.01 nM ($n=20$ sections; 5 mice), 0.1 nM ($n=20$ sections; 5 mice), 10 nM ($n=30$ sections; 5 mice), and 100 nM ($n=30$ sections; 5 mice). Statistical significance was determined using two-tailed Mann–Whitney test. All values are presented in the graphs together with average \pm s.d. **(d)** Annexin V flow cytometry analysis of HPMEC cells treated for 4 h with the indicated doses of PTHLH. Before PTHLH addition, some cells were pretreated for 2 h with the Z-VADfmk caspase inhibitor. In **b** and **d** numbers indicate the average percentages of Annexin-V-positive (apoptotic) cells obtained from three independent experiments where each sample was done in duplicate ($n =$ average of 6 replicates \pm s.d.).

(PTH1R) (Supplementary Fig. 7b), were treated for 24 h with conditioned media from parental and LiM2 cells or PTHLH-deficient LiM2 cells. We found that only the media from cells expressing high levels of PTHLH (LiM2 cells media, 0.02 ± 0.003 nM PTHLH) caused a disruption of the HPMEC monolayer, suggesting that PTHLH induced cell death (Fig. 6a). We corroborated PTHLH contribution to this effect by pre-treatment of the conditioned media with a PTHLH antagonist peptide, which prevented the PTHLH-induced

disruption of the HPMEC monolayer (Supplementary Fig. 7c). Next, we confirmed by Annexin V staining *in vitro* and TUNEL staining *in vivo* that recombinant PTHLH (1–34) was able to induce HPMEC apoptosis in a dose-dependent manner (Fig. 6b,c and Supplementary Fig. 7d). Interestingly, HPMEC apoptosis induced by PTHLH was neither affected by the caspase inhibitor Z-VADfmk (Fig. 6d) nor resulted in PARP or caspase-3 and caspase-7 cleavage (Supplementary Fig. 7e), suggesting that the process was caspase-

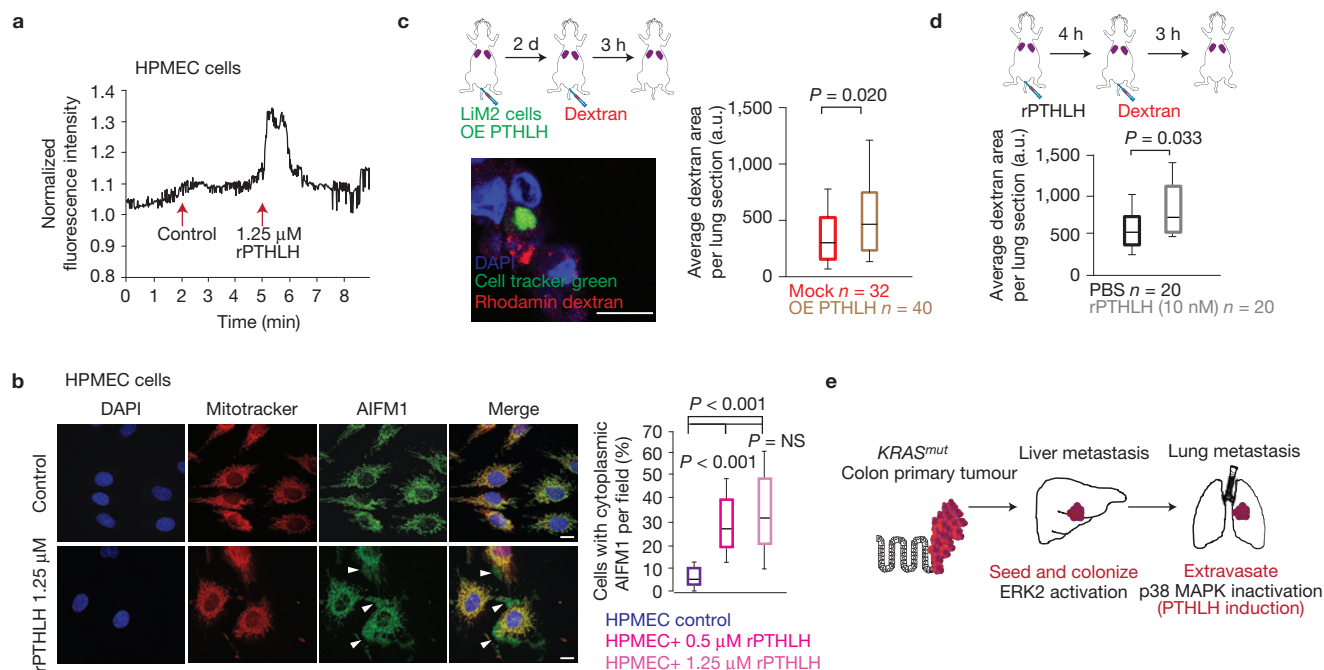


Figure 7 PTHLH induces Ca^{2+} -dependent death of human lung vasculature endothelial cells. **(a)** Relative fluorescence of Fluo4-AM calcium indicator was determined in the course of 9 min. Cells were treated with control medium at 2 min and with medium containing $1.25\ \mu\text{M}$ PTHLH at 5 min. All values were normalized to the lowest value obtained in the first two minutes (basal level). Results represent the average of three independent experiments. **(b)** Left: Representative images from three independent experiments of AIFM1 localization in HPMEC cells treated for 4 h with PTHLH. Arrowheads indicate cytosolic AIFM1. Scale bar, $114\ \mu\text{m}$. Right: Percentage of cells with cytoplasmic AIFM1 from three independent experiments. Each condition was done in duplicate and a total of 10 fields per condition were scored ($n=30$ fields per group). Statistical significance was determined using two-tailed Mann–Whitney test. **(c)** Mice were injected in the tail vein with LIM2 cells mock infected or infected with retrovirus expressing PTHLH. Two days later, rhodamine dextran was injected. Representative image

of staining is presented. Scale bar, $12.5\ \mu\text{m}$. Vascular permeability was measured by determining the average area of rhodamine dextran per lung section using ImageJ software. Eight sections per mouse were analysed. $n=32$ (mock) and $n=40$ (OE PTHLH) total number of sections analysed per group. **(d)** Mice were injected in the tail vein with LIM2 cells treated with or without recombinant PTHLH. Four hours later, rhodamine dextran was injected and vascular permeability was measured by determining the average area of rhodamine dextran per lung section using ImageJ software. Four sections were analysed per mouse and 5 mice per group were used ($n=20$ sections per group). Statistical analysis in **c** and **d** was done using two-tailed Student's *t*-test. **(e)** Schematic representation of p38 MAPK and PTHLH implication in lung metastasis by CRC cells. The box in **b,c** and **d** extends from the 25th to 75th percentile and the black line within the box represents the median; whiskers extend from the 10th to 90th percentile.

independent. Consistent with this possibility, levels of proapoptotic (Bak and Bid) and anti-apoptotic (Bcl-xl and Mcl-1) proteins were not changed on PTHLH treatment (Supplementary Fig. 7f).

PTHLH induces Ca^{2+} -dependent death of endothelial cells of the lung

Previous studies indicated that increased intracellular Ca^{2+} levels can lead to cell death independently of both caspases and Bcl-2 family members^{22,23}. In addition, PTH1R belongs to a group of G-protein-coupled receptors, which on ligand binding can increase Ca^{2+} levels in the cytosol²⁴. Indeed, we found that PTHLH treatment increased Ca^{2+} levels in HPMEC cells (Fig. 7a and Supplementary Video 1). Next, we focused on the apoptosis-inducing factor mitochondrion-associated 1 (AIFM1, also known as AIF), a mitochondrial protein that is thought to play a central role in caspase-independent cell death^{25,26} and that is released from the mitochondria when cytosolic Ca^{2+} levels increase^{22,23}. Interestingly, we observed AIFM1 translocation from the mitochondria to the cytosol on PTHLH treatment (Fig. 7b and Supplementary Fig. 7g). In summary, PTHLH can trigger Ca^{2+} release and AIFM1 mobilization leading to caspase-independent endothelial cell death, which, in

turn, destabilizes the vasculature increasing permeability at the lung metastatic site (Fig. 7c,d). Collectively, these results support that p38 MAPK signalling downregulation couples lung and liver metastasis in *KRAS*-mutant CRC cells through the control of PTHLH expression. The release of PTHLH either from established liver lesions or from metastatic cells trapped at the lung vasculature is likely to increase lung endothelial permeability and facilitate metastatic cells extravasation (Fig. 7e).

DISCUSSION

Our analysis of clinical samples indicates that high levels of ERK2 activity probably drive liver metastasis, whereas low p38 MAPK activity further accounts for the capacity to colonize the lung (Fig. 7e). Moreover, our findings emphasize the ability of the cytokine PTHLH to trigger caspase-independent cell death at the lung vasculature as a previously unrecognized contributor to the hierarchical process of metastasis by facilitating the seeding of the lungs by *KRAS*-mutated CRC cells growing in liver metastatic lesions. Previous studies have implicated PTHLH in breast and squamous cell carcinoma tumour progression to bone metastasis through its activity in the bone remodelling process^{27–29}. Our work illustrates the systemic contribution of

PTHLH released from tumour cells in supporting distant metastatic processes by triggering vascular permeability, and provides an explanation for the enhanced expression of PTHLH reported in CRC tissue compared with normal colorectal mucosa or polyps³⁰. Moreover, our results suggest that genetic changes that allow the primary metastasis to the liver must be followed by additional genetic alterations that allow secondary metastases from the liver to the lung, which emphasizes the concept of metastases from metastases. We provide evidence for a distinct mechanism that relies on different signalling pathways whose hierarchical modulation enhances the ability of departing tumour cells to consecutively seed the liver and the lungs (Fig. 7e). The observation that liver and lung colonization is linked to tumour-specific or circulating cell-specific factors may create opportunities for the development of targeted therapies to prevent disease dissemination from the colon to the liver, and subsequently to the lungs. □

METHODS

Methods and any associated references are available in the [online version of the paper](#).

Note: Supplementary Information is available in the [online version of the paper](#)

ACKNOWLEDGEMENTS

We would like to thank J. Maurel for providing the data on patients with colon and rectal cancers depicted in Supplementary Table 3. We also thank H. Auer, J. Colombelli and M. Gay from the Functional genomics, Microscopy and Mass spectrometry core facilities of IRB Barcelona, respectively. J.U. was supported by Fundación BBVA, a Juan de la Cierva grant from Spanish Ministerio de Ciencia e Innovación (MICINN) and a grant from Fundación Olga Torres. X.G.-A. was supported by Hospital Clinic-IDIBAPS (Ajut a la Recerca Josep Font) and an ASISA-Harvard Fellowship for Excellence in Clinical Research. S.R. was supported by a S. Borrel contract from Instituto de Salud Carlos III. S.G. and M.P. were supported by La Caixa Fellowships and A.B. by FPI from MICINN. R.R.G., E.B. and A.R.N. are supported by the Institut Catalana de Recerca i Estudis Avançats (ICREA). Research support was provided by MICINN (BFU2010-17850), the European Commission FP7 (ERC 294665) and the Fundación BBVA to A.R.N., by the Generalitat de Catalunya (2009 SGR 1437), MINECO P12/01861 and CIBER-BBN NanoCoMets to R.M., and by the Fundación BBVA, AECC, Generalitat de Catalunya (2009 SGR 1429) and MICINN (SAF2010-21171) to R.R.G.

AUTHOR CONTRIBUTIONS

J.U. designed and performed experiments, analysed data and participated in text writing. X.G.-A. designed and established the model system, performed microarrays and participated in text writing and statistical analyses of microarrays and patient data. E.P. performed statistical analyses of patient data. S.R., I.D. and F.M.B. performed experiments and analysed data on p38 MAPK. M.V.C. and R.M. carried out intracaecum injections and analysed the data. A.B. and S.G. contributed to western blots and immunohistochemical analysis. M.G. and M.P. carried out intrasplenic, tail vein and intracaecum injections. E.F. carried out immunohistochemical analysis. C.N. provided and analysed patient data. N.K., E.B. and A.R.N. participated in data analyses and manuscript writing. R.R.G. conceived the project, analysed data, supervised the overall project and wrote the manuscript.

COMPETING FINANCIAL INTERESTS

The authors declare no competing financial interests.

Published online at www.nature.com/doi/10.1038/ncb2977

Reprints and permissions information is available online at www.nature.com/reprints

- Edge, S. B., Byrd, D. R., Compton, C. C. & Fritz, A. G. *AJCC Cancer Staging Manual* (Springer, 2009).
- Gallagher, D. J. & Kemeny, N. Metastatic colorectal cancer: from improved survival to potential cure. *Oncology* **78**, 237–248 (2010).

- Wanebo, H. J. *et al.* Meeting the biologic challenge of colorectal metastases. *Clin. Exp. Metastasis* **29**, 821–839 (2012).
- Sadahiro, S. *et al.* Recurrence patterns after curative resection of colorectal cancer in patients followed for a minimum of ten years. *Hepatogastroenterology* **50**, 1362–1366 (2003).
- Kievit, J. Follow-up of patients with colorectal cancer: numbers needed to test and treat. *Eur. J. Cancer* **38**, 986–999 (2002).
- Nguyen, D. X., Bos, P. D. & Massagué, J. Metastasis: from dissemination to organ-specific colonization. *Nat. Rev. Cancer* **9**, 274–284 (2009).
- Tie, J. *et al.* KRAS mutation is associated with lung metastasis in patients with curatively resected colorectal cancer. *Clin. Cancer Res.* **17**, 1122–1130 (2011).
- Schlüter, K. *et al.* Organ-specific metastatic tumor cell adhesion and extravasation of colon carcinoma cells with different metastatic potential. *Am. J. Pathol.* **169**, 1064–1073 (2006).
- Ding, L. *et al.* Genome remodelling in a basal-like breast cancer metastasis and xenograft. *Nature* **464**, 999–1005 (2010).
- Fidler, I. J. The pathogenesis of cancer metastasis: the 'seed and soil' hypothesis revisited. *Nat. Rev. Cancer* **3**, 453–458 (2003).
- Kaiser, S. *et al.* Transcriptional recapitulation and subversion of embryonic colon development by mouse colon tumor models and human colon cancer. *Genome Biol.* **8**, R131 (2007).
- Smith, J. J. *et al.* Experimentally derived metastasis gene expression profile predicts recurrence and death in patients with colon cancer. *Gastroenterology* **138**, 958–968 (2010).
- Merlos-Suárez, A. *et al.* The intestinal stem cell signature identifies colorectal cancer stem cells and predicts disease relapse. *Cell Stem Cell* **8**, 511–524 (2011).
- Subramanian, A. *et al.* Gene set enrichment analysis: a knowledge-based approach for interpreting genome-wide expression profiles. *Proc. Natl Acad. Sci. USA* **102**, 15545–15550 (2005).
- Wagner, E. F. & Nebreda, A. R. Signal integration by JNK and p38 MAPK pathways in cancer development. *Nat. Rev. Cancer* **9**, 537–549 (2009).
- Cuadrado, A. & Nebreda, A. R. Mechanisms and functions of p38 MAPK signalling. *Biochem. J.* **429**, 403–417 (2010).
- Shin, S., Dimitri, C. A., Yoon, S.-O., Dowdle, W. & Blenis, J. ERK2 but not ERK1 induces epithelial-to-mesenchymal transformation via DEF motif-dependent signaling events. *Mol. Cell* **38**, 114–127 (2010).
- Xing, L. *et al.* Discovery and characterization of atropisomer PH-797804, a p38 MAP kinase inhibitor, as a clinical drug candidate. *Chem. Med. Chem.* **7**, 273–280 (2012).
- Céspedes, M. V. *et al.* Orthotopic microinjection of human colon cancer cells in nude mice induces tumor foci in all clinically relevant metastatic sites. *Am. J. Pathol.* **170**, 1077–1085 (2007).
- Adams, S. L., Cohen, A. J. & Lassová, L. Integration of signaling pathways regulating chondrocyte differentiation during endochondral bone formation. *J. Cell. Physiol.* **213**, 635–641 (2007).
- Hens, J. R. *et al.* BMP4 and PTHrP interact to stimulate ductal outgrowth during embryonic mammary development and to inhibit hair follicle induction. *Development* **134**, 1221–1230 (2007).
- Norberg, E. *et al.* An increase in intracellular Ca²⁺ is required for the activation of mitochondrial calpain to release AIF during cell death. *Cell Death Differ.* **15**, 1857–1864 (2008).
- Sanges, D., Comitato, A., Tammaro, R. & Marigo, V. Apoptosis in retinal degeneration involves cross-talk between apoptosis-inducing factor (AIF) and caspase-12 and is blocked by calpain inhibitors. *Proc. Natl Acad. Sci. USA* **103**, 17366–17371 (2006).
- Vilardaga, J.-P., Romero, G., Friedman, P. A. & Gardella, T. J. Molecular basis of parathyroid hormone receptor signaling and trafficking: a family B GPCR paradigm. *Cell. Mol. Life Sci.* **68**, 1–13 (2011).
- Susin, S. A. *et al.* Two distinct pathways leading to nuclear apoptosis. *J. Exp. Med.* **192**, 571–580 (2000).
- Joza, N. *et al.* Essential role of the mitochondrial apoptosis-inducing factor in programmed cell death. *Nature* **410**, 549–554 (2001).
- Gallwitz, W. E., Guise, T. A. & Mundy, G. R. Guanosine nucleotides inhibit different syndromes of PTHrP excess caused by human cancers *in vivo*. *J. Clin. Invest.* **110**, 1559–1572 (2002).
- Takayama, Y., Mori, T., Nomura, T., Shibahara, T. & Sakamoto, M. Parathyroid-related protein plays a critical role in bone invasion by oral squamous cell carcinoma. *Int. J. Oncol.* **36**, 1387–1394 (2010).
- Guise, T. A. Molecular mechanisms of osteolytic bone metastases. *Cancer* **88**, 2892–2898 (2000).
- Malakouti, S., Asadi, F. K., Kukreja, S. C., Abcarian, H. A. & Cintron, J. R. Parathyroid hormone-related protein expression in the human colon: immunohistochemical evaluation. *Am. Surg.* **62**, 540–544 (1996).

METHODS

Cell culture. The SW620 colorectal cell line was obtained from ATCC. Cells were transduced with retrovirus expressing the triple-fusion reporter gene encoding herpes simplex virus thymidine kinase 1, GFP and firefly luciferase³¹. GFP-expressing cells were sorted and maintained in 5% CO₂ at 37 °C in DMEM medium (Gibco) supplemented with 5% fetal bovine serum (FBS) (Biological Industries), 0.29 mg ml⁻¹ glutamine (Biological Industries), 100 U ml⁻¹ penicillin (Biological Industries) and 0.1 mg ml⁻¹ streptomycin (Biological Industries).

The HCT116 cell line was maintained in DMEM culture medium (Gibco) supplemented with 10% fetal bovine serum (FBS; Biological Industries), 0.29 mg ml⁻¹ glutamine (Biological Industries), 100 U ml⁻¹ penicillin (Biological Industries) and 0.1 mg ml⁻¹ streptomycin (Biological Industries). Clonetics HPMEC cell line was from Promo Cell and was maintained in Endothelial Cell Growth Medium MV2 (Promo Cell). PTHLH (1–34) recombinant protein (H-6630), (Asn 10, Leu 11, D-Trp 12)-PTHLH (7–34) amide antagonist peptide (no. H-3274), rabbit anti-PTHLH (1–34) IgG (no. T-4512) and Z-VADfmk (no. n1560) were purchased from Bachem.

Hyperactivation of the p38 MAPK pathway in HCT116 cells was achieved by stable transfection of MKK6^{EE} cloned into pCDNA3.1(+) using Fugene 6 (Roche), followed by treatment with 100–200 µg ml⁻¹ hygromycin (Invitrogen) for 2 weeks or until death of the non-transfected control. Mock cells were transfected with empty pCDNA3.1(+) and subjected to the same procedure.

Lentiviral production. 293T cells were used for lentiviral production. Lentiviral vectors expressing shRNAs against human *PTHLH*, *MAPK1* (*ERK2*), *MAPK3* (*ERK1*) and *MAPK14* (p38α) from Mission shRNA Library were purchased from Sigma-Aldrich. Transfection of 293T cells with lentiviral vectors was done using standard procedures and viral supernatant was used for infection of SW620 cells. Selection was done using puromycin (2 µg ml⁻¹) for 48 h. As a negative control in all of the infections, lentivirus with non-target shRNA was used (catalogue no. SHC016-1EA).

PTHLH shRNA1 clone ID TRCN0000083846; sequence: 5'-CCGCCAAGATT TA CGGCGACGATCTCGAGAATCGTCGCCGTAAATCTTGGTTTTTG-3'.

PTHLH shRNA2 clone ID TRCN0000083847; sequence: 5'-CCGCGCCGTCGCGA TTTGGGTCTGATCTCGAGATCAGACCCAAATCGGACGGGTTTTTG-3'.

ERK1 shRNA1 clone ID TRCN000006150; sequence: 5'-CCGCCAAGATTT ACGGCGACGATCTCGAGAATCGTCGCCGTAAATCTTGGTTTTTG-3'.

ERK1 shRNA2 clone ID TRCN0000010040; sequence: 5'-CCGGTATACCAA GTCCATCGACATCTCGAGATGTCGATGGACTTGGTATAGTTTTT-3'.

ERK2 shRNA1 clone ID TRCN0000010050; sequence: 5'-CCGGTATCCATTCA GCTAACGTTCTCTCGAGAGAACGTTAGCTGAATGGATATTTTT-3'.

ERK2 shRNA2 clone ID TRCN0000010040; sequence: 5'-CCGGCAAGTTC GAGTAG CTATCAACTCGAGTTGATAGCTACTCGAACTTTGTTTTT-3'.

p38α shRNA clone ID TRCN0000010051; sequence: 5'-CCGGGTACGTGTG CAGTGAAGAAGCTCGAGTTCTTCACTGCCACACGTAACTTTTT-3'.

Animal studies. The institutional Animal Care and Use Committee of IRB Barcelona approved all animal work. BALB/c nude female mice (Harlan) of 6–8 weeks of age were used for all studies.

For intrasplenic injections, animals were anaesthetized with a mixture of ketamine (80 mg kg⁻¹) and xilacine (8 mg kg⁻¹) and 3 × 10⁶ cells resuspended in 100 µl of cold PBS were injected as previously reported³². On injection, cells were allowed for 2 min to pass from the spleen and enter the liver through the portal circulation and next splenectomy was performed. Tumour development was followed twice a week by bioluminescence imaging using the IVIS-200 imaging system from Xenogen. Quantification of bioluminescent images was done with LivingImage 2.60.1 software. For liver metastasis both ventral images of the abdomen and dorsal images of the upper right side of the mice back were quantified. All values were normalized to those obtained at day 0. For metastasis-free survival curves, metastatic events were scored when the measured value of either abdominal or dorsal bioluminescence bypassed the value of day 0. On necropsy, the development of metastasis was confirmed by performing *ex vivo* liver and lung bioluminescent images as well as in histological sections. For tail vein injections 1 × 10⁶ cells were resuspended in 200 µl of cold PBS and injected into the tail vein. Lung tumour development was followed once a week by bioluminescence imaging taking a photo of the upper dorsal region that corresponds to the lung position. Quantification of bioluminescent images was performed with LivingImage 2.60.1 software. All obtained values were normalized to those obtained at day 0. For lung-metastasis-free survival curves, metastatic events were scored when the measured value of bioluminescence bypassed that of day 0. In Fig. 5d, before tail vein inoculation of LIM2-overexpressing PTHLH cells, those were treated with PBS, PTHLH antagonist peptide (AP) ((Asn 10, Leu 11, D-Trp 12)-PTHLH (7–34; Bachem); (5 µg ml⁻¹) and PTHLH-neutralizing antibody (Nab; rabbit anti PTHLH (1–34) IgG; Bachem; 5 µg ml⁻¹). Next, cells were injected through the tail vein and mice were continuously

treated with PBS or PTHLH AP (6 µg per dose, intraperitoneum injection) twice a day or PTHLH NAb (6 µg per dose, intraperitoneum injection) once a day. Lung metastasis was scored as described above.

Orthotopic injections were done as previously described³³. Lung injections were done using 5 × 10⁵ cells that were resuspended in 25 µl of cold PBS mixed with 25 µl of growth factor reduced Matrigel (BD Biosciences, no. 354230). Animals were anaesthetized with a mixture of ketamine (80 mg kg⁻¹) and xilacine (8 mg kg⁻¹). A small incision was made in the skin on the left side of the back of the mouse, level with the lungs, and cells were injected into the lung using a 25G needle. For intraliver injections animals were anaesthetized with a mixture of ketamine (80 mg kg⁻¹) and xilacine (8 mg kg⁻¹). A small incision in the skin and peritoneum was made in the liver area and liver lobules were gently removed. Injections were done using insulin syringes (29Gx1/2 needle) and each mouse was injected with 5 × 10⁵ cells that were resuspended in 25 µl of cold PBS mixed with 25 µl of growth factor reduced Matrigel matrix (BD Biosciences). Liver tumour development was followed once a week by bioluminescence imaging, taking a photo of the ventral region. Quantification of bioluminescent images was performed with LivingImage 2.60.1 software. Once the tumour signal reached an established threshold (>108 photons s⁻¹), mice were randomly allocated to daily oral treatment with 10 mg kg⁻¹ of p38 inhibitor PH-797804 (Selleckchem, no. S2726) or vehicle (0.5% methylcellulose and 0.025% Tween 20 in PBS) for two weeks. For extravasation assays CellTracker Green (Life Technologies, no. C7025)-marked cells (5 × 10⁵) were resuspended in 200 µl of cold PBS and injected into the tail vein. Forty eight hours later mice were perfused by heart with 5 ml of PBS and euthanized. The lungs were removed, the trachea was perfused and these were fixed in formalin. Paraffin-embedded lungs were sectioned and analysed.

For the *in vivo* lung permeability assay, 5 × 10⁵ cells marked with 5 µM CellTracker Green (Life Technologies) were resuspended in 200 µl of cold PBS and injected into the tail vein. Two days after mice were injected intravenously with rhodamine dextran (*M*, 70K, Life Technologies, no. D1841) at 2 mg per 20 g of body weight and 3 h later mice were perfused by heart with 5 ml of PBS and euthanized. The lungs were extracted, the trachea was perfused and these were fixed in formalin. Paraffin-embedded lungs were sectioned and analysed.

In addition, lung permeability was tested on injection of PBS or 10 nM (0.08 µg in 100 µl of PBS) recombinant PTHLH (1–34) through the tail vein. Of note, the molar concentration of rPTHLH was adjusted to 2 ml of the total mouse blood volume. Four hours later, mice were injected intravenously with rhodamine dextran (*M*, 70K, Life Technologies) at 2 mg per 20 g of body weight and 3 h later mice were perfused by heart with 5 ml of PBS and euthanized. The lungs were extracted, the trachea was perfused and these were fixed in formalin. Paraffin-embedded lungs were sectioned and analysed.

For scoring of apoptotic cells in lungs, liver and ovary, PBS and indicated concentrations of rPTHLH were injected through the tail vein of mice. Four hours later mice were euthanized, and tissues were extracted and fixed in formalin.

Isolation of liver metastatic derivatives. Tumour formation on intrasplenic injections was followed by bioluminescence imaging (see above). Mice were euthanized when they presented the first signs of cachexia. Liver metastatic lesions were localized by *ex vivo* bioluminescence imaging and resected under sterile conditions. The lesions were minced and placed in culture medium containing a mixture of DMEM and Ham F-12 (GIBCO) (1:1) supplemented with 0.125% collagenase III and 0.1% hyaluronidase. Samples were incubated at room temperature for 4–5 h, with gentle rocking. After collagenase treatment, cells were briefly centrifuged, resuspended in culture medium and allowed to grow. GFP+ cells were sorted for further propagation in culture or for inoculation in mice.

Gene expression profiling. RNA was extracted from cells using the RNeasy mini kit (Qiagen). Labelling and hybridization of the samples to the HG1.0ST gene expression chip (Affymetrix) were performed by the Functional Genomics Core Facility of IRB Barcelona using standard methodology. Data analysis was performed using R (Bioconductor). Quantile normalization and RMA summarization were used to obtain probe set level expression estimates as implemented in the 'oligo' package of Bioconductor³⁴. Both box plot and MA plots were checked before and after normalization. To prevent nonspecific or mis-targeted probe sets biasing the gene level expression estimates, for each gene we selected the 50% of the probe sets with the highest inter-quartile range across all samples and obtained a gene level expression estimate through median polishing, in a fashion analogous to RMA. Class comparison of differential expression between parental and LIM2 cells was performed with a linear-model-based moderated *t*-test as implemented in the lma package. The *t*-test statistics were used to obtain a posterior probability for differential expression following the semi-parametric empirical Bayes procedure³⁵. The posterior expected false discovery rate was set at 0.05. A heat map was used to plot the expression of genes on a colour scale. A Euclidean distance metric was used to compute the distance matrix of the gene expression levels and hierarchical

clustering using a complete agglomeration method was used. Ranks of the data were used for setting the colour scheme.

GSEA analysis. GSEA analysis was done as implemented in the phenoTest package of Bioconductor.

BGSEA analysis. Gene set enrichment was assessed through Bayesian enrichment³⁶. We generated 1,000 posterior samples for the differential expression indicator, according to the posterior probabilities of differential expression obtained from pairwise comparisons. For each gene set we computed the probability of enrichment as the proportion of posterior samples for which the percentage of differentially expressed genes in the set was larger than the percentage of differentially expressed genes in the rest of the genome.

MKK6 gene expression correlation. Gene expression data of stage II and III patients of the GSE14333 human CRC cohort were used. A Spearman correlation test was performed for each gene against *MKK6* (*MAP2K6*). We corrected for multiple testing using the Benjamini and Hochberg method³⁷.

Migration assay. Cells were marked with 5 μ M CellTracker Green (Life Technologies) following the manufacturer's instructions and kept overnight in medium with 0.1% FBS. The next day 5×10^4 cells were seeded on human-fibronectin-coated Biocoat Cell Culture Inserts (BD Biosciences, no. 354543) in medium with 0.1% FBS, and the wells were loaded with complete medium. Eight hours after the seeding, cells were washed and fixed with 4% paraformaldehyde. Cells on the apical side of each insert were scraped off and the migration to the basolateral side was visualized with a Nikon Eclipse TE2000-U fluorescence microscope.

Trans-endothelial migration assay. HPMEC cells (1×10^5) were seeded on human-fibronectin-coated Biocoat Cell Culture Inserts (BD Biosciences) and allowed to grow for four days until closing the monolayer. Tumour cells were marked with 5 μ M CellTracker Green (Life Technologies) following the manufacturer's instructions and then were conditioned overnight in ECGM-MV2 (Promo Cell) medium with 0.1% FBS and without supplements. The next day 5×10^4 tumour cells were seeded into Trans-well inserts with an endothelial monolayer in ECGM-MV2 medium with 0.1% FBS and the wells were loaded with complete medium. Eight hours after the seeding, cells were washed and fixed with 4% paraformaldehyde. Cells on the apical side of each insert were scraped off and the migration to the basolateral side was visualized with a Nikon Eclipse TE2000-U fluorescence microscope.

Invasion assay. Cells were marked with 5 μ M CellTracker Green (Life Technologies) following the manufacturer's instructions and were kept overnight in medium with 0.1% FBS. The next day, 5×10^4 cells were seeded on BD BioCoat Matrigel Invasion Chambers in medium with 0.1% FBS, and the wells were loaded with complete medium. Eight hours after the seeding, cells were washed and fixed with 4% paraformaldehyde. Cells on the apical side of each insert were scraped off and the migration to the basolateral side was visualized with a Nikon Eclipse TE2000-U fluorescence microscope.

Flow cytometry analysis. 2×10^5 HPMEC cells were seeded in ECGM-MV2 (Promo Cell) complete medium. The following day cells were washed with PBS and treated for 4 h with PTHLH in ECGM-MV2 medium with 0.1%FBS and without supplements. In experiments where Z-VAD-fmk (Bachem) inhibitor was used cells were pretreated for 2 h with this pan-caspase inhibitor before PTHLH was added. Cells were stained with Annexin V Apoptosis Detection Kit (Santa Cruz, sc-4252AK) following the manufacturer's instruction. Data were obtained using a BD FACSAria cell sorter and analysed using FlowJo software.

Western blot analysis. Protein extracts obtained from whole-cell lysates (35 μ g) were fractionated in SDS-PAGE gels, transferred onto Immobilon-P (Millipore) membranes, and subjected to immunoblot analysis according to standard procedures. The following antibodies were used: rabbit polyclonal antibodies to phospho-p38 (Cell Signaling, no. 9211; dilution 1:500), goat polyclonal antibodies against p38 α (Santa Cruz, no. sc-525-G; dilution 1:500), a home-made rabbit antiserum against MKK6 (ref. 38), rabbit monoclonal against phospho-ERK1/2 (Cell Signaling, no. 4377S; dilution 1:500), rabbit polyclonal against ERK1/2 (Cell Signaling no. 9102; dilution 1:500), mouse monoclonal against anti-phospho JNK (BD Transduction Laboratories, no. 612541; dilution 1:500), rabbit polyclonal against JNK (Santa Cruz, no. sc-571; dilution 1:500), rabbit polyclonal against PARP (Cell Signaling no. 9542; dilution 1:500), rabbit polyclonal against caspase-3 (Cell Signaling no. 9662; dilution 1:500), rabbit polyclonal against caspase-7 (Cell Signaling no. 9492; dilution 1:500), rabbit polyclonal against AIF (AIFM1; Cell Signaling no. 4642; dilution 1:500), rabbit polyclonal against Bid (Cell Signaling

no. 2002; dilution 1:1,000), rabbit polyclonal against Bak (Cell Signaling no. 3814; dilution 1:1,000), rabbit monoclonal against Bcl-xl (Cell Signaling no. 2764, clone 54H6; dilution 1:500), rabbit monoclonal against Mcl-1 (Cell Signaling no. 5453, clone D35A5; dilution 1:500) and mouse monoclonal antibody against Tom20 (Santa Cruz, sc-17764, clone F-10; dilution 1:500) and against tubulin (Sigma no. T5168, clone B-5-1-2; dilution 1:5,000).

Primary antibodies were detected with appropriate HRP-conjugated secondary antibodies against mouse (Cell Signaling no. 7076, dilution 1:5,000), rabbit (GE Healthcare UK Limited, no. LNA934V dilution 1:5,000) or goat IgGs (Santa Cruz no. sc-2020, dilution 1:5,000). Separation of cytoplasmic and mitochondrial fractions was done using Mito Isolation Kit for Mammalian Cells (Thermo Scientific) following the manufacturer's instructions.

Quantitative RT-PCR analysis. Real-time qPCR was performed using TaqMan Gene Expression Assay *PTHLH* probe Hs 00174969_m1; *MKK6/MAP2K6* probe Hs00992389_m1 and ABI Prism Fast 7900HT Instrument. The levels of expression were normalized to human B2M (Applied Biosystems) and data were analysed using the comparative Δ CT method.

Histopathology and immunohistochemistry. Tissues were dissected, fixed in 10%-buffered formalin (Sigma) and embedded in paraffin. Sections (2–3 μ m thick) were stained with haematoxylin and eosin (H&E). For immunohistochemistry rat polyclonal rabbit polyclonal antibodies against GFP (Abcam, ab13970; dilution 1:2,000) and P-p38 (Cell Signaling, no. 9211; dilution 1:1,000) were used.

Immunofluorescence. HPMEC cells were grown to confluence on glass coverslips. The cells were fixed for 10 min in 10% neutral buffered formalin solution (Sigma) at room temperature and incubated for 5 min in 0.1% Triton X-100 in PBS. Next, the samples were blocked with 1% BSA for 30 min and then stained for 20 min with rhodamine phalloidin (Life Technologies, no. R415) and DAPI (Sigma).

For AIF staining 5×10^4 of HPMEC cells were seeded on glass coverslips. The next day, cells were treated for 4 h with 1.25 mM PTHLH in 0.1%FBS ECGM-MV2 (Promo Cell) medium without supplements and stained with 80 nM MitoTracker Red CMXRos (Lonza no. PA3017) for 15 min. Next, cells were fixed in complete growth medium containing 3.7% formaldehyde for 15 min at 37 °C and permeabilized for 10 min in PBS containing 0.2% Triton X-100. Blocking was done in PBS containing 3% BSA for 1 h at room temperature. Samples were incubated with AIF (AIFM1) antibody (Cell Signaling no. 4642; dilution 1:100) overnight at 4 °C and 1 h at room temperature with secondary antibody that recognizes rabbit IgGs (Alexa Fluor 488, Molecular Probes Invitrogen) and mounted with ProLong Gold antifade reagent with DAPI.

For PTHLH immunofluorescence LiM2 and PTHLH-overexpressing LiM2 cells were seeded on glass coverslips. Next, cells were fixed with 4% PFA for 15 min at room temperature and permeabilized for 10 min in PBS containing 0.2% Triton X-100. Blocking was performed in PBS containing 3% BSA for 1 h at room temperature. Samples were incubated with PTHLH antibody (Abcam Ab115488; dilution 1:100) overnight at 4 °C and 1 h at room temperature with secondary antibody that recognizes mouse IgGs and mounted with ProLong Gold antifade reagent with DAPI.

PTHLH ELISA assay. For the ELISA assay, 36.4 μ g of total protein lysate was used. ELISA was purchased from Uscn Life Science (USA) and performed following the manufacturer's instructions.

TUNEL assay. For the TUNEL assay formalin-fixed paraffin-embedded sections were used. *In Situ* Cell Death Detection Kit was purchased from Roche and assay was used following the manufacturer's instructions.

Live-cell imaging for intracellular Ca²⁺ level detection. HPMEC cells (3×10^5) were seeded on 14 mm glass coverslips. The next day, cells were washed and treated for 15 min with 1 μ M Fluo-4 AM (Life Technologies, no. F14201) in ECGM-MV2 medium without supplements. Next, the cells were mounted in a special chamber for live-cell imaging using a ScanAR Olympus microscope and images were taken every second. Obtained videos were analysed using Fiji software.

Human samples. Informed consent was obtained prospectively before surgery from each patient and a total of 23 primary tumours and healthy mucosa were obtained. Patient identifiers were removed from the samples to protect patient confidentiality as per institutional guidelines. All human samples were manipulated with the approval and following the guidelines of the Ethic Committee of Hospital Clinic de Barcelona and IRB-Barcelona. Information on tumour relapse and follow-up was extracted from the medical records; patients were followed with CT scan every three months. Owing to the lack of material 3 samples could be subjected only to mRNA isolation whereas the rest were subjected to both mRNA and protein isolation.

Clinical sample analysis. Authorization was obtained to analyse a database of 100 metastatic colorectal cancer (CRC) patients treated with irinotecan and cetuximab inside a phase II translational trial³⁹ and 40 localized patients from a single cohort prospective study⁴⁰ that relapsed during the study follow-up. Site of metastasis was extracted and tabulated by primary site (colon versus rectum) with basic descriptive statistics.

Mass spectrometry analysis. Proteins were digested with trypsin following standard protocols. Briefly, 50 µg of sample was reduced with 2 mM dithiothreitol. After 1 h at 25 °C, iodoacetamide was added to a final concentration of 7 mM and the samples were incubated for 30 min in the darkness. The reaction was stopped by adding 2 mM dithiothreitol. Then, proteins were digested with trypsin and incubated at 37 °C overnight. Digestions were stopped by adding formic acid to a final concentration of 1%. The resulting peptide mixtures were diluted in 1% FA and loaded in a nano-LC-MS/MS system. The nano-LC-MS/MS set up was as follows. Samples were loaded to a 180 µm × 2 cm C18 Symmetry trap column (Waters) at a flow rate of 15 µl min⁻¹ using a nanoAcquity Ultra Performance LCTM chromatographic system (Waters). Peptides were separated using a C18 analytical column (BEH130TM 75 µm × 10 cm, 1.7 µm, Waters) with a 90 min run, comprising three consecutive steps with linear gradients from 1 to 35% B in 60 min, from 35 to 50% B in 5 min, and from 50% to 85% B in 3 min, followed by isocratic elution at 85% B in 10 min and stabilization to initial conditions (A = 0.1% FA in water, B = 0.1% FA in CH₃CN). The column outlet was directly connected to an Advion TriVersa NanoMate (Advion) fitted to an LTQ-FT Ultra mass spectrometer (Thermo). Spray voltage in the NanoMate source was set to 1.70 kV. Capillary voltage and tube lens on the LTQ-FT were tuned to 40 V and 120 V. The spectrometer was working in positive polarity mode. At least two blank runs before each analysis were performed to ensure the absence of cross-contamination from previous samples. To select the PTHLH-targeted ions, the mass spectrometer was operated in a data-dependent acquisition (DDA) mode. Survey MS scans were acquired in the FT with the resolution (defined at 400 *m/z*) set to 100,000. Up to six of the most intense ions per scan were fragmented and detected in the linear ion trap. The ion count target value was 1,000,000 for the survey scan and 50,000 for the MS/MS scan. Target ions already selected for MS/MS were dynamically excluded for 30 s. A database search was performed with Proteome Discoverer software v1.3 (Thermo) using the Sequest search engine and the SwissProt database (human release 12_03) where PTHLH peptide was added. Search parameters included trypsin enzyme specificity, allowing for two missed cleavage sites, carbamidomethyl in cysteine as a static modification and methionine oxidation as dynamic modifications. Peptide mass tolerance was 10 ppm and the MS/MS tolerance was 0.8 Da. Peptides with a *q* value lower than 0.1 were considered as positive identifications with a high confidence level. One peptide ion was selected for targeted MS/MS analysis: SDQDLR (*m/z* 366.21). The presence of PTHLH in the samples was determined by using the same nano-LC-MS/MS system described above. The spectrometric analysis was performed in a targeted mode, acquiring a full MS/MS scan of the precursor ion SDQDLR (*m/z* 366.21). The quantification was performed with Xcalibur software versus 2.0SR2 (Thermo Scientific) by using extracted ion chromatograms of the optimum MS/MS transitions in terms of sensitivity (SDQDLR, 366.22 → 531.38).

Sample size calculation. An assessment of the number of animals required for each procedure was performed using Statistical Power Analysis and taking into consideration the appropriate statistical tests, significance level of 5% and statistical power of 80%. An estimate of variance was inferred from previous experiments, especially considering the variability of tumour xenograft growth.

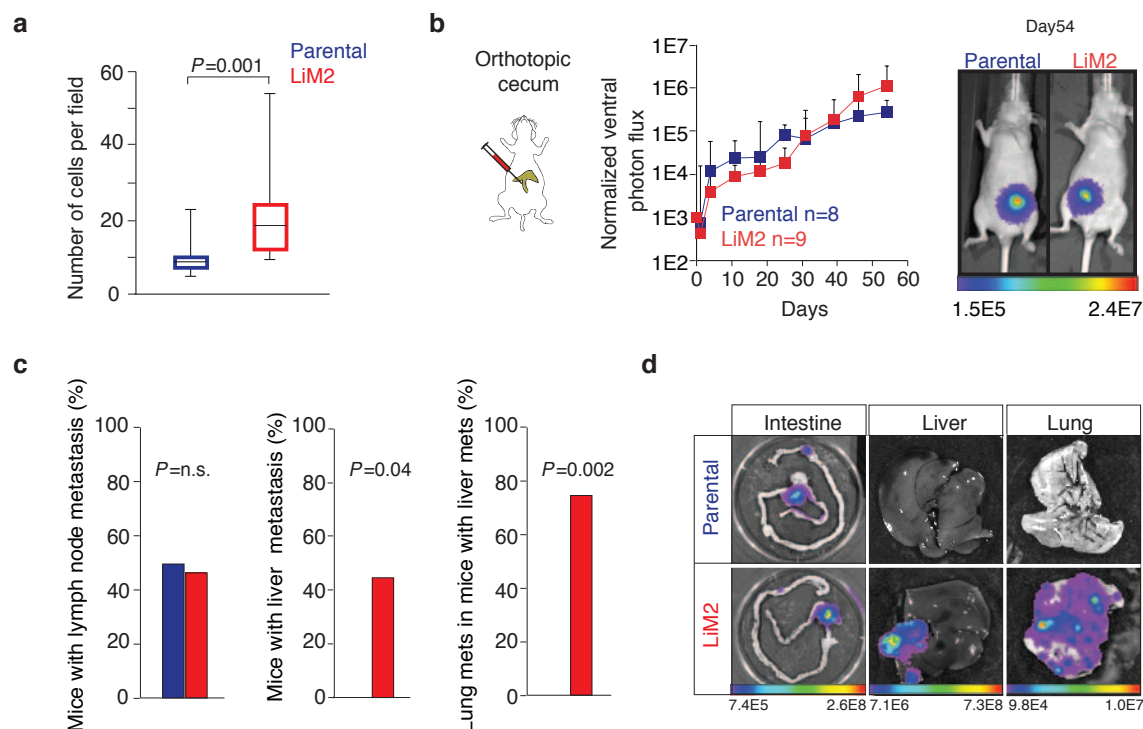
Method of randomization. A method of randomization was used in the experiment shown in Fig. 3c. Parental cells were implanted directly into the liver in nude mice (one implant per mouse) and, when the liver tumour signal reached a certain photon flux threshold (> 1 × 10⁸ photons s⁻¹), mice were randomly allocated to daily systemic treatment with either vehicle or PH-797804.

Group allocation. For the results obtained in Figs 5e, 6c and 7c,d and Supplementary Figs 1a, 3d,e, 4b,e,f and 7a,d the investigator was not aware of group allocation when assessing the outcome.

Data sets analysed. GSE17538 is a metacohort composed of 177 colon cancer patients treated at H. Lee Moffitt Cancer Center (Tampa, USA) plus 55 colon cancer patients treated at Vanderbilt University Medical Center (Vanderbilt, USA; ref. 41). Note that this cohort did not include rectal cancers. GSE14333 contains a pool of 290 CRC patients treated at two different hospitals: Peter MacCallum Cancer Center (Australia) and H. Lee Moffitt Cancer Center (USA; ref. 42). We combined both cohorts for a total of 340 CRC expression data sets from which we used 267 (stages I, II and III). Note that the GSE17538 and GSE14333 cohorts were partially overlapping owing to patients treated at H. Lee Moffitt Cancer Center being duplicated in both data sets. Duplicated cases were included only once in the final selection. To remove biases due to the data having been collected in different hospitals, we computed *z*-scores (that is, subtracted the mean and divided by the standard deviation) for each gene and hospital separately before merging them into a meta-cohort.

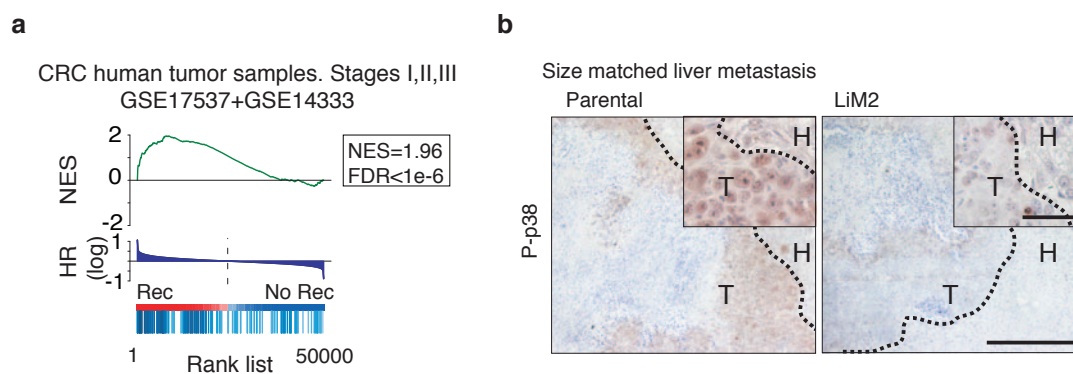
Accession number of data set generated for this study (Fig. 2a): GSE33350.

31. Ponomarev, V. *et al.* A novel triple-modality reporter gene for whole-body fluorescent, bioluminescent, and nuclear noninvasive imaging. *Eur. J. Nucl. Med. Mol. Imaging* **31**, 740–751 (2004).
32. Giavazzi, R., Campbell, D. E., Jessup, J. M., Cleary, K. & Fidler, I. J. Metastatic behavior of tumor cells isolated from primary and metastatic human colorectal carcinomas implanted into different sites in nude mice. *Cancer Res.* **46**, 1928–1933 (1986).
33. Céspedes, M. V. *et al.* Orthotopic microinjection of human colon cancer cells in nude mice induces tumor foci in all clinically relevant metastatic sites. *Am. J. Pathol.* **170**, 1077–1085 (2007).
34. Gentleman, R. C. *et al.* Bioconductor: open software development for computational biology and bioinformatics. *Genome Biol.* **5**, R80 (2004).
35. Rossell, D., Guerra, R. & Scott, C. Semi-parametric differential, expression analysis via partial mixture estimation. *Stat. Appl. Genet. Mol. Biol.* **7**, Article15 (2008).
36. Mallick, B. K., Gold, D. & Baladandayuthapani, V. *Bayesian Analysis of Gene Expression Data* (Wiley, 2009).
37. Benjamini, Y. & Hochberg, Y. Controlling the false discovery rate: a practical and powerful approach to multiple testing. *J. Roy. Stat. Soc. Ser. B* **57**, 289–300 (1995).
38. Alonso, G., Ambrosino, C., Jones, M. & Nebreda, A. R. Differential activation of p38 mitogen-activated protein kinase isoforms depending on signal strength. *J. Biol. Chem.* **275**, 40641–40648 (2000).
39. Garcia-Albeniz, X. *et al.* Serum matrilysin correlates with poor survival independently of KRAS and BRAF status in refractory advanced colorectal cancer patients treated with irinotecan plus cetuximab. *Tumour Biol.* **32**, 417–424 (2011).
40. Martínez-Fernández, A. *et al.* Serum matrilysin levels predict outcome in curatively resected colorectal cancer patients. *Ann. Surg. Oncol.* **16**, 1412–1420 (2009).
41. Smith, J. J. *et al.* Experimentally derived metastasis gene expression profile predicts recurrence and death in patients with colon cancer. *Gastroenterology* **138**, 958–968 (2010).
42. Jorissen, R. N. *et al.* Metastasis-associated gene expression changes predict poor outcomes in patients with dukes stage B and C colorectal cancer. *Clin. Cancer Res.* **15**, 7642–7651 (2009).



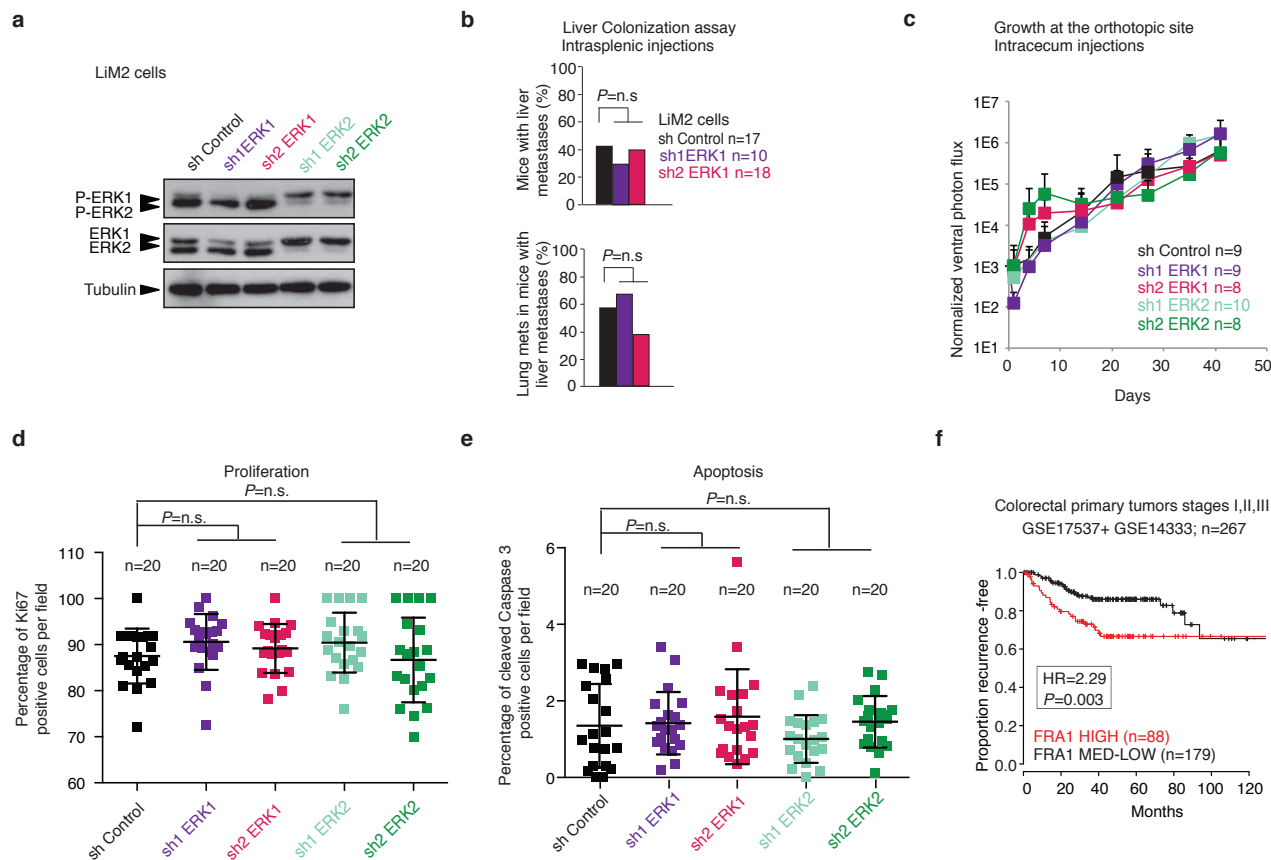
Supplementary Figure 1 Characterization of liver and lung metastatic potential of SW620 parental and LiM2 cells. **(a)** Invasion capacity of SW620 parental and LiM2 cells was measured using matrigel-coated Boyden chambers. Results represent values of three independent experiments where each cell line was seeded in six Boyden chambers and five fields per chamber were analyzed and average for each chamber obtained (n=18 chambers per group). Statistical significance was calculated using two-tailed Mann Whitney test; the box extends from 25 to 75 percentile where black line within the box represents median, whiskers extend from 10 to 90 percentile. **(b)** *In vivo* proliferation of parental and LiM2 cells (0.5×10^5) injected into cecum of nude

mice. Bioluminescent images were taken at day 54. n =8 (Parental) and n=9 (LiM2) number of mice used for each cell line. Statistical analysis was done using two-tailed Mann Whitney test and no statistically significant differences were found. **(c)** Percentage of lymph node and liver metastasis as well as lung metastasis in mice that developed liver metastasis upon intracecum injections of parental and LiM2 cells determined post-mortem. Number of mice (n) used is defined in (b). Statistical significance was calculated using one-sided Fisher's exact test. **(d)** Representative bioluminescent images of intestine, liver and lung from mice injected intracecum with SW620 parental and LiM2 cells. Data is presented as average plus s.d.



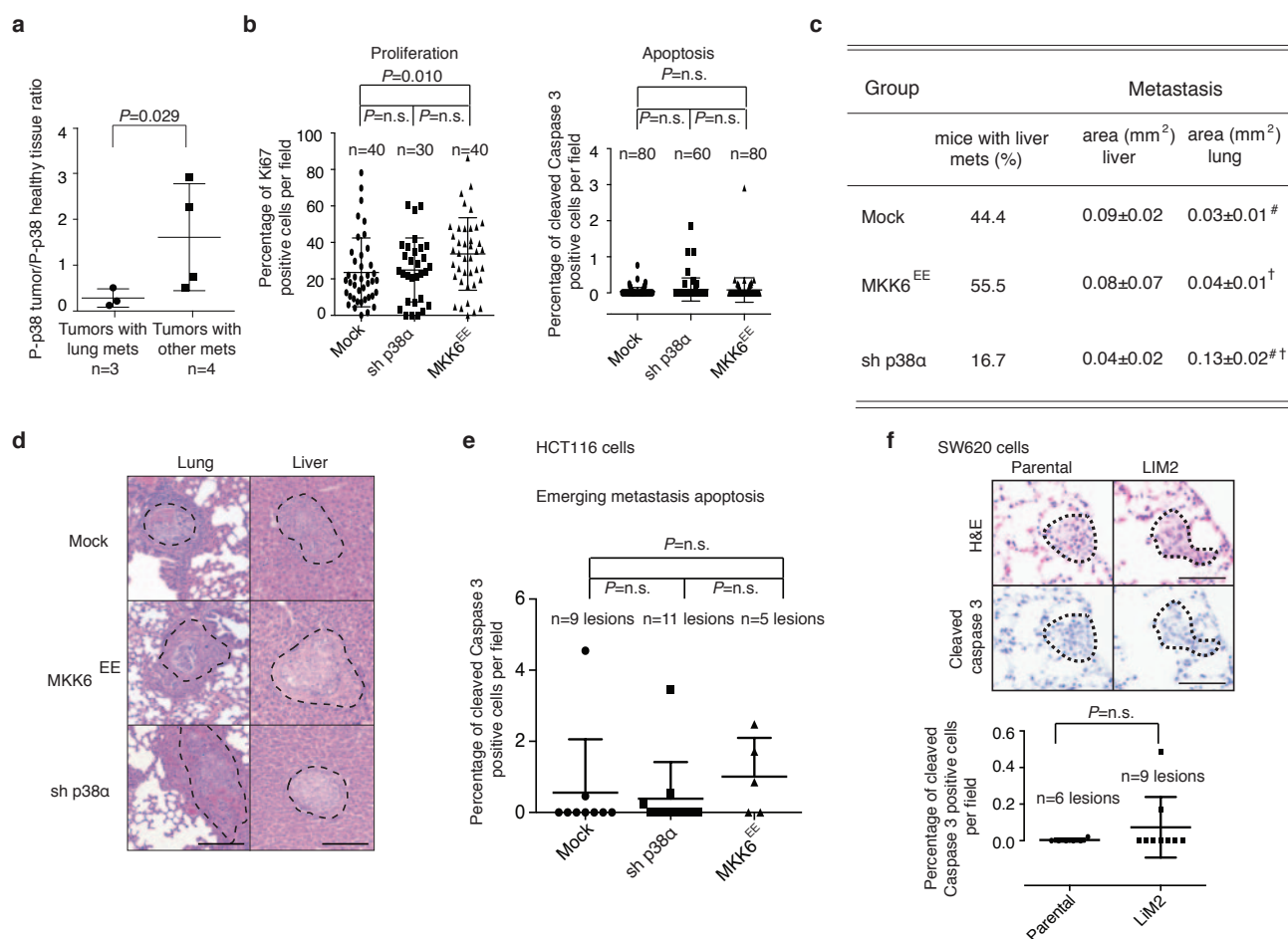
Supplementary Figure 2 Gene set enrichment analyses (GSEA) of the CCM downregulated gene set and phosphorylated p38 MAPK levels in liver metastatic lesions formed by LiM2 cells. **(a)** GSEA analysis of the CCM downregulated gene set in human colon cancer dataset (pooled GSE17537 and GSE14333 expression set). NES-normalized enrichment score; FDR-false

discovery rate. **(b)** SW620 parental and LiM2 cells were injected intraliver and 40 days later mice were sacrificed. Size matched liver lesions were selected for immunohistochemistry staining with anti-phospho-p38 (P-p38) antibodies. Representative IHC staining is shown where $n=6$ animals per group were used. Scale bar 500 μm ; inset scale bar 50 μm ; H-healthy tissue; T-tumor.



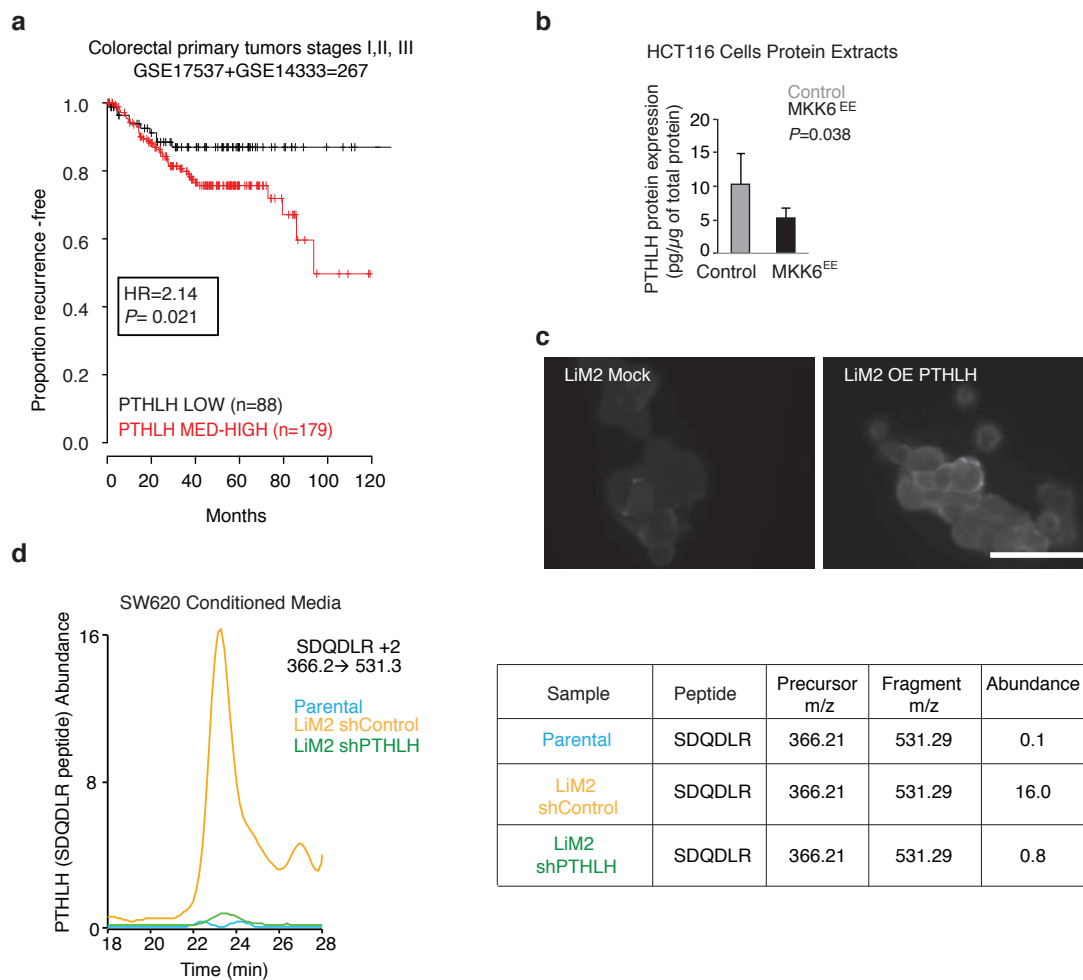
Supplementary Figure 3 ERK1 and ERK2 influence on primary tumors and metastasis. **(a)** ERK1 and ERK2 downregulation was confirmed by Western blotting (representative Western blots from three independent experiments are shown). **(b)** Percentage of mice intrasplenically injected with LiM2 cells expressing the indicated shRNAs that developed liver metastases (up) or lung metastasis (bottom). n= 17 (shControl), n=10 (sh1 ERK1) and n=18 (sh2 ERK1) number of mice used per group pooled from two independent experiments. Statistical analysis was done using two-sided Fisher's exact test. n.s.- not significant. **(c)** LiM2 cells expressing the indicated shRNAs were injected orthotopically into mice cecum and growth rates by photon flux quantification were determined. n=9 (shControl), n=9 (sh1 ERK1), n=8 (sh2 ERK1), n=10 (sh1 ERK2), n=8 (sh2 ERK2) number of mice used per group.

Data is presented as average plus s.d. Statistical analysis was done using one-way ANOVA and no statistical differences were found. **(d and e)** Size matched lesions from (c) were selected for immunohistochemistry Ki-67 (d) and cleaved caspase-3 staining (e). n=20 total fields per group analyzed where five different fields from size matched lesions per mouse were quantified. Number of mice used in each group was 4. Statistical analysis was done using two-tailed Mann Whitney test. All values are presented in the graphs together with average \pm s.d. **(f)** Kaplan-Meier curves representing association of proportion of recurrence-free patients with relative *FRA1* gene expression levels in human primary colon cancer dataset (pooled GSE17537 and GSE14333; n=267). HR-hazard ratio. Statistical analysis was done using Cox proportional hazard's model.



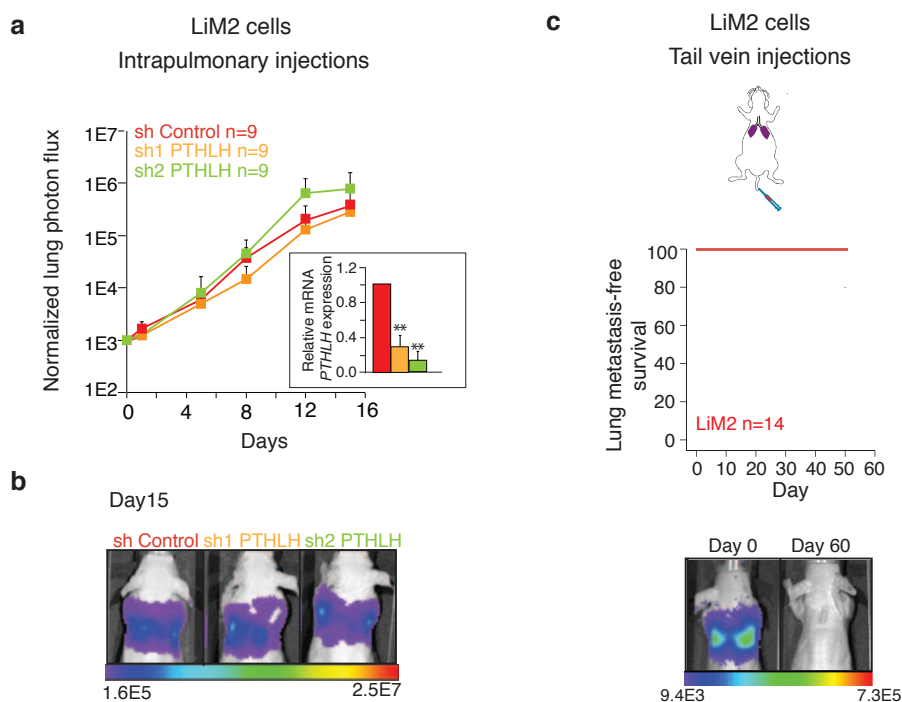
Supplementary Figure 4 Lung metastasis in colon cancer associates with low levels of phospho-p38 MAPK in primary tumors. **(a)** Association of lung metastasis with levels of phosphorylated p38 (P-p38) protein in samples of 7 primary CRC tumor samples that developed metastasis. P-p38 levels were normalized to p38 total amount of protein and P-p38 expressed in the respective healthy mucosa samples. $n=3$ tumors with lung mets and $n=4$ tumors with other mets. Statistical analysis was done using one-tailed Mann Whitney test. **(b)** HCT116 cells expressing p38 α shRNAs or constitutively active MKK6^{EE} were injected orthotopically into mice cecum and size matched lesions were selected for Ki-67 and cleaved caspase-3 staining. Five different fields per lesion and mouse for Ki67 staining and ten different fields /lesion/mouse for cleaved caspase-3 staining were scored. $n=40$ (Mock), $n=30$ (sh p38 α) and $n=40$ (MKK6^{EE}) total number of fields per group analyzed for Ki67 staining. $n=80$ (Mock), $n=60$ (sh p38 α) and $n=80$ (MKK6^{EE}) total number of fields per group analyzed for cleaved caspase-3 staining. **(c)** HCT116 cells expressing p38 α shRNAs or constitutively active MKK6^{EE} were injected orthotopically into mice cecum and the percentage of

mice that developed liver metastasis, the area of liver and lung metastasis were determined. #, † indicate the groups which statistically significant. # $P=0.001$; † $P=0.017$. Values for area represent mean \pm s.e.m. $n=41$ (Mock), $n=14$ (sh p38 α) and $n=61$ (MKK6^{EE}) number of lung lesions analyzed. **(d)** Representative H&E staining of lung and liver histological sections from (c). Dashed lines delineate metastasis. Scale bar 200 μ m. **(e)** Emerging lung metastatic lesions from HCT116 cells expressing p38 α shRNAs or constitutively active MKK6^{EE} injected orthotopically into mice cecum were selected for cleaved caspase-3 staining. $n=9$ (Mock), $n=11$ (sh p38 α) and $n=5$ (MKK6^{EE}) total number of lesions analyzed per group. **(f)** Emerging lung metastatic lesions from SW620 parental and LiM2 cells were selected for cleaved caspase-3 staining. $n=6$ (Parental) and $n=9$ (LiM2) total number of lesions analyzed per group. Scale bar 50 μ m. For (b), (c), (e) and (f) two-tailed Mann Whitney test was used for statistical analysis; n.s.- not significant. In panels (a), (b), and (f) all values are presented in the graphs together with average \pm s.d. In panel (e) all values are presented in the graph together with average plus s.d.



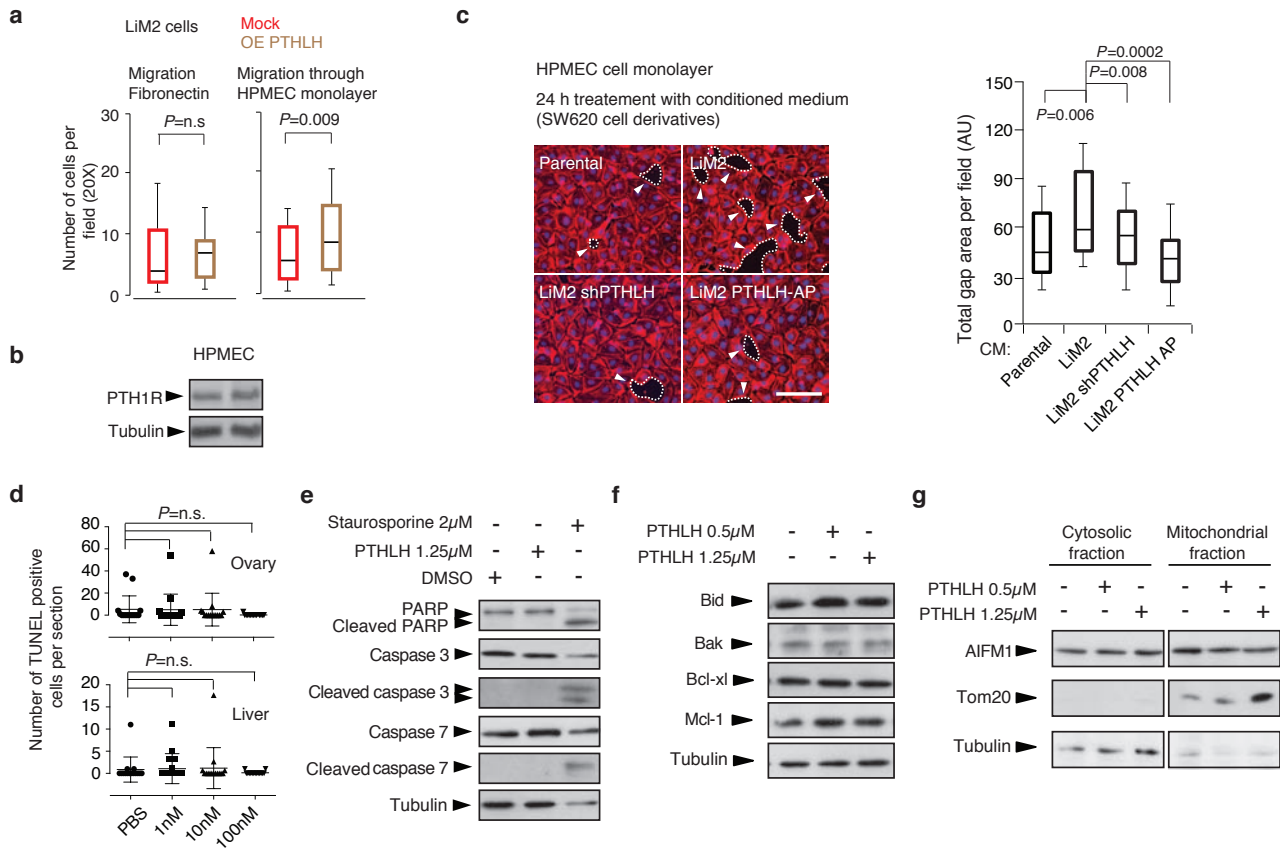
Supplementary Figure 5 *PTHLH* gene expression is associated with poor clinical outcome in patients with colon cancer. **(a)** Kaplan-Meier curves representing association of proportion of recurrence-free patients with relative *PTHLH* gene expression levels in human primary colon cancer dataset (pooled GSE17537 and GSE14333; n=267). HR-hazard ratio. Statistical analysis was done using Cox proportional hazard's model. **(b and c)** ELISA analysis of *PTHLH* levels in HCT116 cells (n=3 values from

independent experiments) expressing constitutively active MKK6EE (b) or immunofluorescence analysis of *PTHLH* levels (representative images from two independent experiments) in SW620 cells expressing *PTHLH* (c). Statistical analysis was done using one-tailed Student's t test in (b) and graphs represent average plus s.d. Scale bar in (c) 50µM. **(d)** Detection of *PTHLH* by mass-spec analysis in conditioned medium from SW620 parental, LiM2 shControl and LiM2 shPTHLH cell lines.



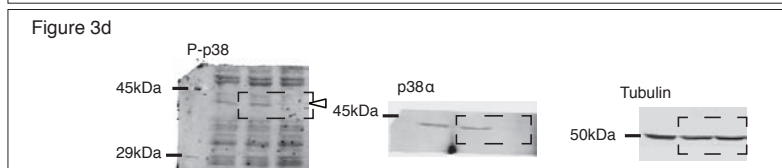
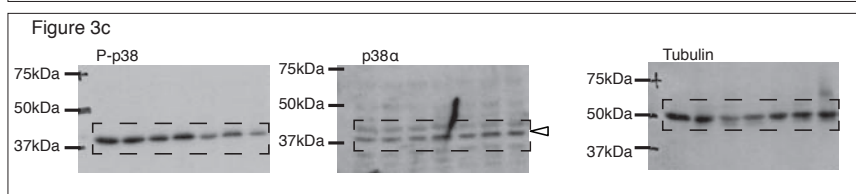
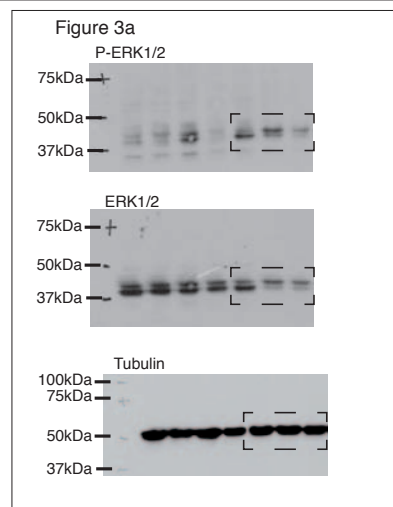
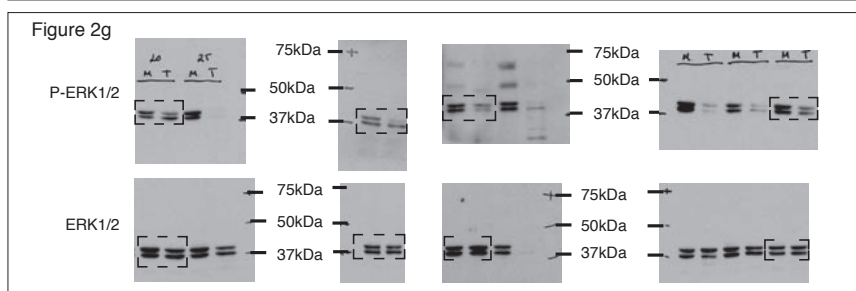
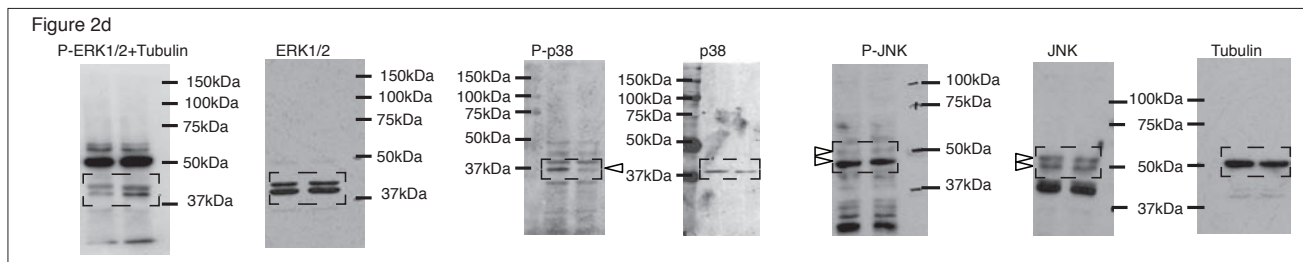
Supplementary Figure 6 *PTHLH* does not affect the growth of LiM2 cells in the lung. **(a)** Photon flux of dorsal upper back area of mice injected intrapulmonary with LiM2 cells expressing two different shRNA against *PTHLH*. Normalization was done to values of day 0. n=9 (sh Control), n=9 (sh1 *PTHLH*) and n=9 (sh2 *PTHLH*) number of mice used per group. Inset represents qRT-PCR analysis of *PTHLH* expression levels in LiM2 cells infected with lentivirus expressing shRNA against *PTHLH* or the control shRNA in three independent experiments (n=3). Statistical analysis for

main graph was done using two-tailed Mann Whitney test and no statistically significant differences were found. Statistics for the graph presented in inset was done using two-tailed Student's t test. ** $P < 0.001$. Values represented in the main graph as well as in inset represent average plus s.d. **(b)** Representative bioluminescent images of mice injected intrapulmonary with LiM2 cells expressing two different shRNAs against *PTHLH*. **(c)** Lung metastasis-free survival of mice (n = 14) upon tail vein injection of LiM2 cells. Representative bioluminescent images are shown.

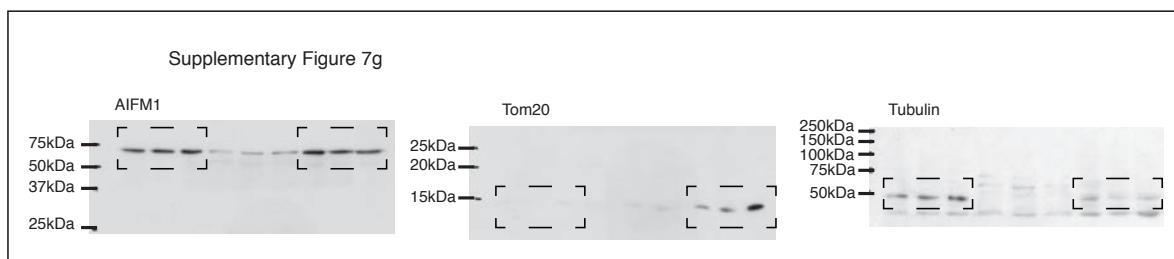
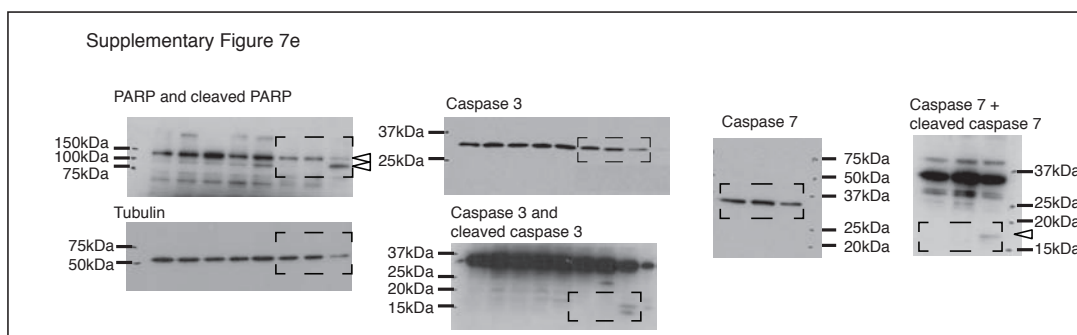
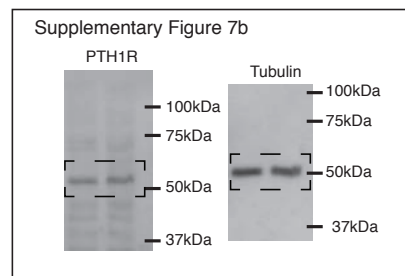
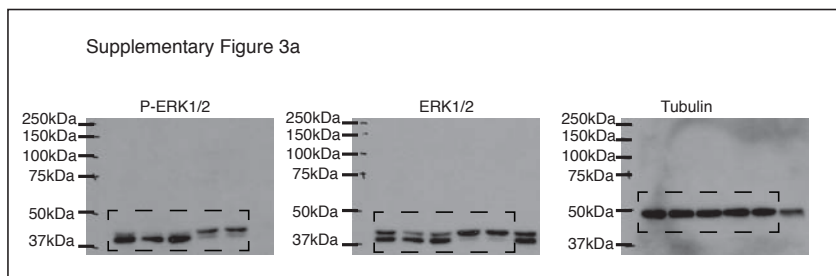


Supplementary Figure 7 Effect of PTHLH on endothelial cells of the lung. **(a)** Migration of LiM2 cells mock infected or infected with a retrovirus that expresses PTHLH was scored in Boyden chambers covered with fibronectin or with fibronectin and HPMEC monolayer. Each cell line was seeded in triplicate and 5 fields per chamber were counted. Results represent three independent experiments for migration through fibronectin and four independent experiments for migration through fibronectin and HPMEC monolayer. $n=45$ total number of fields analyzed per group for migration through fibronectin and $n=60$ total number of fields analyzed per group for migration through fibronectin and HPMEC monolayer. Statistical analysis was done using two-tailed Mann Whitney test **(b)** Western blot analysis of PTH1R expression levels in HPMEC cells (representative images from two independent experiments). Tubulin was used as a loading control. **(c)** HPMEC cells were grown until reaching tight confluence and then were treated for 24 h with conditioned medium from SW620 parental, LiM2, LiM2 shPTHLH and LiM2 treated cells with PTHLH-Antagonist Peptide (AP). Phalloidin staining was performed and total gap area per field was determined. Results represent values of three independent experiments where each sample was seeded in duplicate and for each coverslip at least 5 fields were analyzed. $n=40,40,40$ and 30 total number of fields analyzed per group respectively. Statistical

analysis was done using two-tailed Student's t test; scale bar 100 μ m. **(d)** Average number of TUNEL-positive cells in ovary or liver 4 h post tail vein injection of recombinant PTHLH (1-34). Three 30 μ m distant sections per animal were counted. PBS, 1 nM, 10 nM, and 100 nM rPTHLH (5 mice per group). $n=15$ total number of sections analyzed per group. Statistical analysis was done using two-tailed Mann Whitney test; n.s.-not significant. All values are presented in the graphs together with average \pm s.d. **(e)** Western blot analysis of total and cleaved PARP, Caspases-3 and Caspases-7 in HPMEC cells treated for 20 h with PTHLH or Staurosporine. Tubulin was used as a loading control. **(f)** Western blot analysis of pro-apoptotic and anti-apoptotic protein levels in HPMEC cells upon 4 h treatment with the indicated doses of recombinant PTHLH. Tubulin was used as a loading control. **(g)** HPMEC cells were treated for 4 h with the indicated doses of recombinant PTHLH and the cytosolic and mitochondrial fractions were isolated and subjected to western blot analysis for AIFM1 protein expression levels. Tom 20 was used as a loading control of mitochondria and tubulin as a loading control of cytosol. In panels (a) and (c) the box extends from 25 to 75 percentile where black line within the box represents median, the whiskers extend from 10 to 90 percentile. Western blot images in (e), (f) and (g) are representative from at least two independent experiments.



Supplementary Figure 8 Full scans



Supplementary Figure 8 continued Full scans

Supplementary Video Legend

Supplementary Video 1 PTHLH treatment increases intracellular Ca²⁺ levels. Cells were treated for 15 min with Fluo4-AM calcium indicator and then imaged for 9 min. First two minutes of imaging were used for determining the basal Ca²⁺ levels. At min 2, control media was added to cells and at min 5 media with 1.25µM recombinant PTHLH.

Supplementary Table Legends

Supplementary Table 1 Genes differentially expressed between Parental and LiM2 cells. Comparative genome-wide expression analysis of genes that were overexpressed or underexpressed at least 2.5-fold in the highly liver metastatic derivative LiM2 compared to parental cells

Supplementary Table 2 BGSEA for KEGG gene sets (Parental vs. LiM2). By using BGSEA we identified pathway-specific gene expression signatures (KEGG gene sets) that were differentially represented in the gene expression profiles of parental and LiM2 cells.

Supplementary Table 3 Frequency of liver and lung metastasis in a pooled analysis of patients with metastatic colon and rectal cancers. Frequency of liver and lung metastasis in a pooled analysis of patients with metastatic colon and rectal cancers with clinical annotation for the site of metastasis.

Supplementary Table 4 Genes differentially expressed in LiM2 cells compared to Parental that correlated significantly with MKK6 expression in CRC primary tumors. Genes differentially expressed in LiM2 cells compared to Parental ($f_c > 1.7$) that correlated significantly ($p < 0.05$) with MKK6 expression in Stage II and III CRC primary tumors.